catalysts

MDPI

Review

Process Simulation for the Design and Scale Up of Heterogeneous Catalytic Process: Kinetic Modelling Issues

Antonio Tripodi [1], Matteo Compagnoni [1], Rocco Martinazzo [1], Gianguido Ramis [2] and Ilenia Rossetti [1,*]

1 Dipartimento di Chimica, Università degli Studi di Milano, CNR-ISTM and INSTM Unit Milano-Università, I-20133 Milan, Italy; antonio.tripodi@unimi.it (A.T.); matteo.compagnoni@unimi.it (M.C.); rocco.martinazzo@unimi.it (R.M.)

2 Dipartimento di Ingegneria Chimica, Civile ed Ambientale, Università degli Studi di Genova and INSTM Unit Genova, I-16029 Genoa, Italy; gianguidoramis@unige.it

* Correspondence: ilenia.rossetti@unimi.it; Fax: +39-02-50314300

Academic Editor: José R. B. Gomes

Received: 18 March 2017; Accepted: 10 May 2017; Published: 18 May 2017

Abstract: Process simulation represents an important tool for plant design and optimization, either applied to well established or to newly developed processes. Suitable thermodynamic packages should be selected in order to properly describe the behavior of reactors and unit operations and to precisely define phase equilibria. Moreover, a detailed and representative kinetic scheme should be available to predict correctly the dependence of the process on its main variables. This review points out some models and methods for kinetic analysis specifically applied to the simulation of catalytic processes, as a basis for process design and optimization. Attention is paid also to microkinetic modelling and to the methods based on first principles, to elucidate mechanisms and independently calculate thermodynamic and kinetic parameters. Different case studies support the discussion. At first, we have selected two basic examples from the industrial chemistry practice, e.g., ammonia and methanol synthesis, which may be described through a relatively simple reaction pathway and the relative available kinetic scheme. Then, a more complex reaction network is deeply discussed to define the conversion of bioethanol into syngas/hydrogen or into building blocks, such as ethylene. In this case, lumped kinetic schemes completely fail the description of process behavior. Thus, in this case, more detailed—e.g., microkinetic—schemes should be available to implement into the simulator. However, the correct definition of all the kinetic data when complex microkinetic mechanisms are used, often leads to unreliable, highly correlated parameters. In such cases, greater effort to independently estimate some relevant kinetic/thermodynamic data through Density Functional Theory (DFT)/ab initio methods may be helpful to improve process description.

Keywords: process simulation; kinetic modelling; ammonia; methanol; bioethanol; steam reforming; ethylene

---

1. Introduction: How to Implement Kinetic Models into Process Simulators

The implementation of kinetic models into process simulators is a scientific and industrial field in continuous growth. Process simulators allow the detailed design of chemical processes with the direct comparison of different scenarios: alternative process layout, size, connection between process streams, and equipment are allowed. Through these instruments, it is possible to size and optimize processes in a relatively fast way. The examples here reported were mainly drawn by considering a commercial process simulator, Aspen Plus, but the same holds for other products available in the market.

When introducing a reactor in a flowsheet, different reactor options become available. The stoichiometric and yield reactors require some definition of the reactions taking place and their extent (e.g., in form of yield of different products). This is easily applied to experimental result, but it does not allow to tune freely the process variables, since their influence on reactor performance is missing. Equilibrium or Gibbs reactors are useful to define the dependence on process variables, but consider the reactor working at equilibrium, so reactor sizing is not allowed. In this case, the size will be undefined, but sufficient to achieve equilibrium conversion. Finally the batch, plug-flow (PFR, in case filled with catalyst) and continuous stirred tank (CSTR) reactors are the most flexible options, which allow a full description of the process under variable conditions and proper sizing of the reactor. However, to perform these calculations, a suitable reaction set and the relative kinetic model and thermodynamic data must be defined.

Reactor models for continuous flow reactor sizing in Aspen Plus® also allow to compute pressure drop across the reactor, typically through the Ergun equation, and are suitable to describe multibed or multitubular reactors accomplishing direct heat exchange between different process streams. This is useful e.g., to define internal heat recovery between hot and cold streams. Catalyst effectiveness factor can also be accounted for, in order to precisely define possible internal mass transfer limitations in the catalyst bed. A different level of detail is possible, but it is usually not possible to account for backdiffusion in axial direction or to compute the radial concentration profiles. In some cases, these points may be implemented developing user-made subroutines as an embedded Fortran code (*vide infra*). The interested reader is referred to detailed work on computational fluid dynamics (CFD), where the description of reactants and catalyst interaction can be accounted for with the desired level of detail. However, the core of the sizing of chemical reactors remains the availability of a detailed kinetic model.

Kinetics of heterogeneous catalytic reactions represents a delicate field, due to the several factors involved. The catalyst belongs to a different phase with respect to the reactants, thus besides the reaction step, adsorption and desorption stages should be added, increasing the complexity of modeling. The easiest model available is the power rate law model, which formally takes care of adsorption by using appropriate apparent reaction orders. Although suitable in some cases, this model is too empirical to be generalized for process simulation. The observed kinetic constant and reaction orders should include the dependence on adsorption/desorption phenomena, which can depend differently on process parameters than the intrinsic kinetic constant. For this reason, a Langmuir–Hinshelwood–Hougen–Watson (LHHW) model is preferably adopted, which more adequately computes the adsorption and desorption steps, which possibly limit the reaction rate. Selected scientific papers are reported below in order to explore representative case studies as examples of implementation of kinetic parameters in a process simulation software to simulate heterogeneous catalytic processes.

The logical workflow of this review is therefore the following, addressing different issues with an increasing complexity scheme:

(1) Process simulation is a key step for process design;
(2) Reactive systems need the definition of a reaction set with the relative kinetic parameters in a well standardized form, essentially the same for the different process simulators;
(3) For some relatively simple, yet very important systems, the literature available on kinetic description is already suitable for a direct implementation into the process simulator (examples are reported in the following for ammonia and methanol synthesis);
(4) When kinetic models are not available in this form, suitable kinetic data should be regressed again in the needed form for implementation in the process simulator;
(5) In case particular kinetic equations are specifically needed, differing from the LHHW model, user models can be implemented in external subroutines and recalled by the simulator;
(6) When the reaction set complexity becomes too high, lumped kinetic models are no more useful, because the powerful aid of the simulator is the prediction of plant performance under

widely varied conditions. Empirical models are also at risk from this point of view. Therefore, microkinetic modelling allows the simulator to reliably follow the system performance;

(7) Again, if the amount of parameters to be determined in a microkinetic scheme becomes too high, high correlation among them is usually observed and predictions reliability is newly at risk. Therefore, especially in such cases, the possibility of independently determining some of the required kinetic parameters through ab initio methods is a powerful tool to cope with this issue.

In this context, this review provides some guidelines to implement heterogeneous catalytic systems into process simulators, dealing with different, increasingly complex, kinetic approaches. We will mainly describe steady state simulations, except for some papers which discuss process control issues, based on dynamic models. Irrespectively on this, kinetics must be provided in the same form. In the following paragraphs, different approaches to implement kinetic models in process simulators are described, following an increasing complexity order. So, in Section 2, complex reaction networks will be presented, together with some examples of first principles aided methods to derive kinetic and thermodynamic parameters for this scope.

1.1. Methanol Synthesis

Methanol synthesis is one of the most studied reactions from both the chemical and the engineering points of view. A detailed study to assess the economic optimization of a methanol synthesis plant was presented by Luyben [1]. The investigation confirmed that the economics were dominated by methanol yield, therefore the availability of reliable kinetic data was fundamental in order to correctly size the plant. The chemistry of the methanol synthesis involves the reaction of both carbon dioxide and carbon monoxide with hydrogen. The author implemented in Aspen Plus the kinetic model and parameters obtained by Bussche and Froment [2] using a LHHW-type equation, able to describe with good precision the reactions of methanol production and the Reverse-WGS reaction.

$$CO_2 + 3H_2 \leftrightarrows CH_3OH + H_2O \tag{R1}$$

$$CO_2 + H_2 \leftrightarrows CO + H_2O \tag{R2}$$

The LHHW kinetic model is constituted by a kinetic factor (in the simplest cases equal to the kinetic constant, more in general depending on it), a driving force expression (depending on the reactants available in the reaction medium) and an adsorption term, weighting the reactants truly available on catalyst surface, which may be much lower than those present in gas/liquid phase (Equation (1)).

$$r = \frac{(\text{kinetic factor})(\text{driving force})}{\text{adsorption term}} \tag{1}$$

The kinetic factor can be expressed as

$$kinetic\ factor = \mathrm{A}\ T^{n} \mathrm{e}^{-\mathrm{E}_a/\mathrm{RT}} \tag{2}$$

where A is the preexponential factor in the Arrhenius expression, E_a is the activation energy and it is possible to express a further dependence from temperature through the exponent n, which, however, is often set to zero. Alternatively, it is possible to refer the temperature dependence of the kinetic constant in comparison to a reference temperature T_0, at which the value k_0 of the kinetic constant is known

$$kinetic\ factor = k_0 \left(\frac{T}{T_0}\right)^{n} e^{(-\mathrm{E_a}/\mathrm{R})\left(\frac{1}{T} - \frac{1}{T_0}\right)} \tag{3}$$

The 'driving force' factor expresses the available amount of the reactants in fluid phase, each with its own reaction order, considering the forward and possible reverse reactions (the latter with negative sign). It takes the following form, where K_1 and K_2 represent equilibrium constants, and K_1 is often set to 1

$$driving\ force = K_1 \prod C_i^{\alpha} - K_2 \prod C_i^{\beta} \tag{4}$$

The term referred as 'adsorption' must be entered as

$$adsorption = \sum K_i \left(\prod C_j^{\gamma} \right) \tag{5}$$

where K_i represents the adsorption constants of each species.

The concentration basis for the driving force and adsorption terms is fugacity powered to the concentration exponents for forward and backward reactions (these are named terms 1 and 2 in Aspen Plus®), respectively. The equilibrium and adsorption constants must be implemented in the following form to compute their dependence on temperature

$$\ln K = \mathrm{A} + \frac{B}{T} + C \ln T + DT \tag{6}$$

Therefore, if different expressions are available for the different kinetic or thermodynamic parameters, they have to be regressed again to meet the formulation required by the simulation software and to explicitly cope with the variable conditions that will be met during the simulation. For the introduction of this type of kinetics in the process simulator, it is necessary to define the reaction rate in kmol s^{-1} m^3 if it is calculated on the volume of reactor, or in kmol s^{-1} $kg^{-1}{}_{cat}$ if it is normalized with respect to the weight of catalyst. This in accordance with the design equation chosen for the plug flow or packed bed reactor under study.

The kinetic data proposed by Bussche and Froment [2] expressed pressures in bar and reaction rates in kmol min^{-1} $kg^{-1}{}_{cat}$. The reader is advised to carefully check the consistency of the units required by the simulator, making reference to the online guides available and to properly convert the units as exemplified by Van Dal et al. [3].

The reactor was simulated using the RPLUG model with a 'constant medium temperature' as the dynamic heat transfer selection. This kind of reactor is the best choice to simulate plug flow configuration with composition changing along the reactor length (or catalyst mass), since it allows the full definition of kinetics and, hence, the prediction of reactor output under widely different conditions. The kinetic equation involves the integration of appropriate composition and rate terms along the reactor profile.

Another key factor is the proper definition of models to estimate the thermodynamic and transport properties of each pure component and of the whole mixture. The presence of substantial errors in the estimation of such properties can lead to major problems in both sizing and rating. A wide choice of thermodynamic packages exists, which can be grouped into three main groups: the ideal model (the simplest of all, it does not consider molecular interactions or size), the models based on activity coefficients to compute non-ideality in liquid phase (Van Laar, Wilson, NRTL, etc.), possibly coupled with equations of state (EOS) to account for non-ideality of the gas, and the models based on equations of state for every phase (SRK, Peng-Robinson, Predictive-SRK, etc.). The Soave–Redlich–Kwong (SRK) equation of state was applied for instance by Bussche and Froment [2], but Luyben [1] did not explicitly state the model used in the simulation. This equation is able to represent both liquid and vapor phases in condition far from the ideality, which is the case of this high pressure process.

A similar work on kinetic implementation in process simulation software was carried out by Van-Dal and Bouallou, although the starting feed was not syngas, but hydrogen and carbon dioxide captured from flue gases [3]. The kinetic model considered was the same proposed by Bussche and Froment with readjusted parameters. In this case, the equations for the thermodynamic equilibrium were incorporated into the kinetic constants. The pressure drop in the fixed bed was calculated through the Ergun equation. Aspen Plus allows proper fields for computing the pressure drop across packed-bed reactors in Plug Flow configuration and packed-bed pipes. It is possible also to add a pressure drop scaling factor (multiplication factor used to correct the pressure-drop computed from the frictional correlations) and roughness of the reactor wall.

Zhang et al. implemented a different kinetic expression for the gas to methanol process, obtained by the combination of the surface reaction of a methoxy species, the hydrogenation of a formate intermediate HCO_2 and the WGS reaction [4,5]. The occurrence of possible internal pore diffusional limitation was determined on the basis of the Weisz-Prater criterion and the effective diffusivity for multicomponent mixture was calculated. A conceptual design tightly related to the economic analysis of the process was performed, revealing the highest economic impact of the methanol reactor. This further shed light on the importance of correct kinetic modeling and its implementation in the simulator. The Peng–Robinson (PR) equation of state was selected as the thermodynamic model, which guarantees accurate calculation results in modelling light gases, alcohols, and hydrocarbons. Generally, the PR equation provides results similar to those of the SRK equation, although it is better to predict the densities of many components in the liquid phase, especially those that are non-polar.

Matzen and co-workers studied the methanol production using renewable hydrogen and CO_2 [6]. The SRK method was adopted to estimate the properties of the mixture with gaseous compounds at high temperature and pressure, and the NRTL-RK model for the methanol column to better represent the vapor/liquid equilibrium between methanol and water. This is an important feature, allowed in Aspen Plus, i.e., the possibility to select the most appropriate model in different sections of the flowsheet. The reactor was simulated as a packed bed reactor with a counter-current thermal fluid. Also, in this case, a LHHW model was adopted.

The investigation and comparison of kinetic and the thermodynamic approach was performed by Iyer et al. [7]. For the kinetic side a plug flow reactor was adopted, implementing the LHHW model and the parameters suggested by Bussche and Froment [2]. In Aspen Plus software this reactor model is a tubular reactor with or without packed catalyst, where perfect mixing is assumed in the radial direction, but not in the axial one. It enables the inclusion of coolant which flows counter-current or in parallel, and it requires knowledge of reaction kinetics. For the thermodynamic study, a Gibbs reactor model was adopted, which calculates chemical and phase equilibrium by minimizing the Gibbs-free energy, even without specifying any reactions. This module differs from the equilibrium reactor model, which instead calculates the thermodynamic equilibrium by a stoichiometric approach and with suitable thermodynamic data. Comparison of kinetic with thermodynamic model revealed the key effect of feed composition on the performance of methanol synthesis for isothermal and adiabatic operation under single and two phase conditions.

Therefore, comprehensive and sufficiently complete kinetic data are available to model the performance of a methanol synthesis reactor. This enables building an improved process design and process optimization by using a relatively simple kinetic scheme.

1.2. Ammonia Synthesis

Another fundamental process with extremely large scale production is the ammonia synthesis. A considerable number of papers focus on catalyst development and kinetic modelling. The implementation in a process simulation software represents a key step to develop new ammonia catalysts and to optimize this technology, as a key to market.

A detailed investigation of the ammonia synthesis mechanism was carried out on promoted Ru/C catalysts under industrially relevant conditions (T = 370–460 °C; P = 50–100 bar) [8–11]. The microkinetic model was based on a modified Temkin equation with the addition of both H_2 and NH_3 adsorption terms, in order to consider the inhibiting effect of hydrogen on catalyst performance [8]. This is a major difference between Ru-based catalysts, which are inhibited by hydrogen, and the commercial Fe-based ones, which are inhibited by the product, ammonia, and substantially unaffected by the reactants. It is clear that a correct comparison between these two different catalytic systems should be done under different conditions. For instance, the Fe-containing catalyst works optimally when feeding the stoichiometric mixture (H_2/N_2 = 3 mol/mol), whereas substoichiometric feed is preferable for Ru (e.g., H_2/N_2 = 1–1.5 mol/mol). On the contrary, the commercial magnetite catalyst rapidly reaches a plateau conversion, due to the fact that increasing ammonia concentration decreases the reaction rate, which is not the case for Ru-based catalysts. This may suggest the development of multibed reactors, with intercooling, using the Fe-based catalyst in the first layers and Ru (more expensive) in the last one, only, to achieve the higher conversion unattainable with Fe. Process simulation and optimization of reactor design and operating conditions are currently in progress by our group, implementing the kinetic parameters in Aspen Plus. The work was planned after a thorough screening of the literature surprisingly revealed a lack in combining kinetic experiments with simulation software. Then a proper simulation of the best industrial technology available using Ru catalyst was carried out (namely the KAAP technology). The reactor is composed of three beds (the first one based on iron while the others based on ruthenium), represented for the simulation as three different plug flow reactors with intermediate cooling (Figure 1).

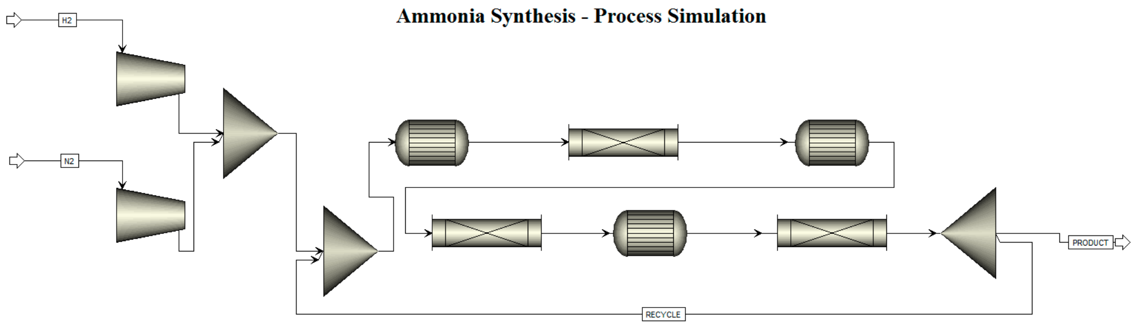

Figure 1. Flowsheet of a multibed reactor for ammonia synthesis.

Yu et al. tried to implement the kinetic parameters of ammonia synthesis for the evaluation of a coal-based polygeneration process to coproduce synthetic natural gas and ammonia [12]. Unfortunately, the way the kinetic parameters were implemented in the simulation was not detailed, probably for conciseness in the economy of the work, which was a complete design and economic evaluation from air and coal to ammonia and electric energy production. Many design variables were investigated, considering the total annual cost. Concerning the reactor, the total annual cost decreased as the system pressure increased, because the enhanced density and thermodynamic driving force decreased the required reactor volume and the catalyst loading, overcoming the higher cost of compression.

At the opposite side, Arora and co-workers investigated a small scale ammonia production from biomass [13]. The flowsheet implies the biomass gasification through a dual fluidized bed gasifier configuration for the production of syngas, which is then purified from CO_x by pressure swing adsorption (PSA) and methanation. An air separation unit provides pure nitrogen and the ammonia reactor produces the ammonia stream. The Redlich-Kwong-Soave, corrected by Boston Mathias (RKS-BM) thermodynamic package was used to model the entire flowsheet. This property package is suitable for processes that involve non-polar and real components, such as gas production, gas processing, and hydrocarbon separation. Gibbs and equilibrium reactors were used to model the ammonia converter. This choice was properly motivated considering that the reaction usually approaches the equilibrium conversion. However, this point should be considered more in detail. The model was validated against some plant data reported in literature.

Ammonia production via integrated biomass gasification was studied by Andersson and Lundgren [14]. The process simulator was used to model energy and material balances of the complete biomass gasification system including the NH_3 synthesis. The most important modelling constraint was the fixed pulp production at a given value and consequently the process stream balance. Also, in this case the reactor was simulated using a Gibbs reactor at 180 bar and 440 °C, formally using an iron promoted catalyst.

A control structure design for the ammonia synthesis process was carried out by Araujo and Skogestad [15]. The reactor configuration was based on an industrial fixed-bed autothermal reactor. The reaction kinetic was described by the Temkin–Pyzhev expression and the beds were modelled in Aspen Plus by means of its built-in catalytic plug-flow reactor. The evaluation of the effectiveness of a control structure against disturbance was carried out using the dynamic simulation package.

Therefore, considering ammonia synthesis, apparently a limited number of papers deal with the optimization of process design and its intensification based on process simulation. Of these, some deal with equilibrium reactors, *de facto* neglecting catalyst role. Improvement on this side is allowed by the availability of readily usable kinetic models with full and detailed parameters, to be used as a basis for simulation. This point is becoming increasingly important due to the spreading interest on ammonia decomposition plants, of limited scale, to achieve pure hydrogen for cogeneration units based on fuel cells. Therefore, reliable tools for multiscale process optimization are straightforward instruments.

1.3. Effect of Transport Phenomena

Diffusion in porous solids is another key factor to compute, because of the possibly controlling mass transfer during the heterogeneous catalytic process. This point must be taken into account and properly implemented in the simulator software considering where necessary the bulk or Knudsen modes of diffusion in small pores. This problem occurs not only in heterogeneous catalytic process, but also in classical gas–solid reactions. For instance, Mahinpey and co-workers studied the CO_2 capture technology using several calcium oxide sorbent materials [16]. The trend of CO_2 adsorption and reaction was simulated by Aspen Plus, matching the experimental results obtained in parallel experiments. A plug flow reactor was adopted as carbonator reactor, while a Gibbs reactor was chosen for the comparison with the thermodynamic equilibrium conditions. A marked difference between the predictions and the conversion derived from the experimental data was observed and attributed to the grain model used for the calculation of the reaction parameters. The possibility that internal points of the sorbent were never touched by the reactant gas was not taken into proper account by e.g., modelling the concentration profile across the catalyst particle and this led to the discrepancy. The authors suggested that a proper optimization can be done considering these not accessible zones.

This point remains one of the most critical for a detailed computation of the process. A trade off should be found between the development of detailed models which take into account fluid dynamics, internal and external mass transfer as limiting for kinetics, and usability of such models. A detailed microkinetic scheme can also be used in this field, but typically this is limited to the description of single unit operations, becoming computationally too heavy to allow implementation in a full plant simulation. Hybrid, semiempirical factors, in the form of efficiencies can be used to take into account all the factors limiting kinetics.

1.4. User Defined Models

Another approach must be adopted for processes which cannot be simulated. One of the most representative example in literature is the biomass gasification in dual fluidized bed reactor [17]. This technology includes two reactors in series: the gasifier where biomass is converted by steam into syngas (H_2 + CO) and a combustion reactor fed with sand and char able to supply thermal energy to the former. None of the commercial process simulators (Aspen Plus, ProII, Hysys, etc.) have predefined models to simulate biomass gasification. Therefore, the kinetic model must be implemented in external files, elaborated with proper software such as MATLAB or powerful scientific programming tools such as Fortran. Abdelouahed et al. exploited the flexibility of Aspen Plus inserting several Fortran blocks, combining complex reactor models and Aspen Plus® tools [17]. Reactor modelling can be done by empirical correlations (product yields as a function of temperature), chemical kinetics, or more detailed reactor computations. The output of the flowsheet preceding the reactor simulated by Aspen Plus® (mass and enthalpy flow rates, temperature, pressure, etc.) is transferred to Fortran modules for the detailed calculation of reactor output through a more or less detailed model, and then transferred back to Aspen (Figure 2). The possibility to implement user defined models makes the difference between the various process simulators. Indeed, the flexibility of the process simulator is measured in terms of the possibility to use kinetic models of any form, which are considered more adequate to represent the studied reaction with respect to the standard models implemented by default in the software.

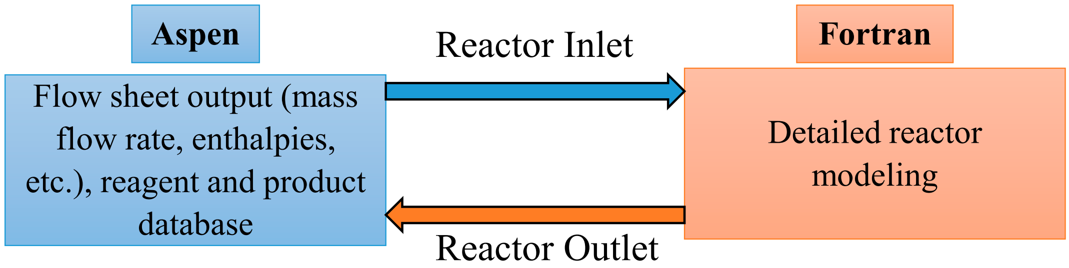

Figure 2. Conceptual block diagram: coupling Aspen Plus® flowsheet with external Fortran modules (readapted from Abdelouahed et al. [17]).

2. Processes Following Complex Kinetic Schemes

From the above reported examples, the need of a sound kinetic model to compute the reactants/products evolution under different reaction conditions appears as a must to be fulfilled for reliable predictions of reactor (and hence process) outcome. As the complexity of the reactions carried out in the process increases, this becomes one of the key issues to be settled prior to process design. In the following, we will consider the emblematic case of ethanol valorization into hydrogen or ethylene, as a pathway to the biorefinery exploitation [18–21]. In this view, a biomass-derived raw material is used to provide important chemicals/fuels in a more sustainable way. This idea has to prove sustainable from the industrial and economical points of view, therefore process simulation is a powerful tool for preliminary process design, to evaluate the operating conditions and process layout that may ensure the economical viability of the process. Process simulation has been carried out e.g., to evaluate the performance of a 5 $kW_{electrical}$ + 5 $kW_{thermal}$ cogeneration unit starting from bioethanol and converting the reformate by means of fuel cells [22–25].

At difference with the cases reported in the previous paragraphs, in this case the complexity of the kinetic scheme increases abruptly. On one hand we do not have only one/two reactions, well independent, to be implemented in the simulator reaction set, but also a complex reaction network including many different parallel/consecutive reactions. On the other hand, kinetic data for such reaction networks can be hardly achieved in reliable way. Indeed, often data regression ends in strongly correlated parameters, which is ultimately unreliable for safe predictions. Therefore, in such cases the use of independent first principles methods for the estimation of some of them lightens and uncorrelates the remaining parameters to be regressed. These topics will be addressed in the following paragraphs by using some examples.

2.1. *Simulations of Reforming Processes*

Hydrogen Production by Steam Reforming

Steam reforming (SR) is more and more studied to produce hydrogen from either fossil or renewable sources. Ethanol is one of the most widely used substrates among the renewable ones. In order to enhance the hydrogen yield avoiding the direct ethanol combustion, only water should be considered as an additional feedstock, without oxygen. Dry Reforming (DR) of methane, in turn, is often operated in such conditions as to make methane a relatively stable species, which is often converted in separated reaction stages: SR and DR followed by methanation (MET) then originates two different reforming process [26]. Starting from a first-principle thermodynamic analysis and keeping in mind this difference, the equilibrium mixtures arising from a given feed composition can be calculated at least in three ways: (1) any species possibly originated from SR, DR, water gas shift (WGS) and methane conversion (occurring simultaneously) is quantified according to its Gibbs free energy; (2) only chemicals are considered originated from ethanol SR plus WGS (methane not present, as it were fully converted in the same step); (3) from DR, with full conversion of ethanol into CH_4 and CO in a pre-reformer, followed by a separate WGS and MET equilibration stage.

The results are shown schematically in Table 1. The calculations originally performed with PROII [26] have been replaced with similar ones performed in Aspen Plus—the same reactor type and SRK thermodynamic model were used. Notice that the calculation scheme shown in Figure 2 of the cited work may not rigorously treat the formation of coke, since two equilibration stages are shown, but only one is modeled via a Gibbs reactor, while nothing is specified about the capability of other PROII reactor classes to mix solid and vapor phases. The differences in these thermodynamic material balances are due to the different setup of the equilibrium reactor blocks in each case, which is the easiest way to account for the catalysts selectivity in a real flow-scheme (where the simultaneous reaction equilibria can be effectively separated in practice).

Table 1. Equilibrium composition (mol/mol_{tot}) of a mixture derived from ethanol reforming under the assumptions specified above; in case 3, water is fed separately to the second reactor (rather than being treated as inert in the first block).

T (°C)	Molar Fractions at 1 Atm (Feed: H_2O:Ethanol = 5:1)											
	Case 1				Case 2				Case 3			
	H_2	CO/CO_2	CH_4	Coke	H_2	CO/CO_2	CH_4	Coke	H_2	CO/CO_2	CH_4	Coke
500	0.30	0.13	0.10	0.00	0.0	0.20	0.00	0.09	0.30	0.13	0.10	0.00
600	0.45	0.50	0.03	0.00	0.52	0.69	0.00	0.00	0.45	0.50	0.03	0.00
700	0.49	0.99	0.00	0.00	0.50	1.02	0.00	0.00	0.49	0.99	0.00	0.00
800	0.48	1.40	0.00	0.00	0.48	1.40	0.00	0.00	0.48	1.40	0.00	0.00
900	0.47	1.82	0.00	0.00	0.47	1.82	0.00	0.00	0.47	1.82	0.00	0.00
1000	0.46	2.25	0.00	0.00	0.46	2.25	0.00	0.00	0.46	2.25	0.00	0.00

The two basic Ethanol SR and DR flowsheets are reproduced in Figure 3 (adapted from [26]). The Product-to-Feed auto-heat exchange is the usual solution when dealing with and endothermic reaction (that requires a pre-heating) which gives byproducts that are still hot enough and if they are not fully oxidized, then can also be used as an additional fuel to sustain the needed heat input, economizing fresh and higher-value fuels.

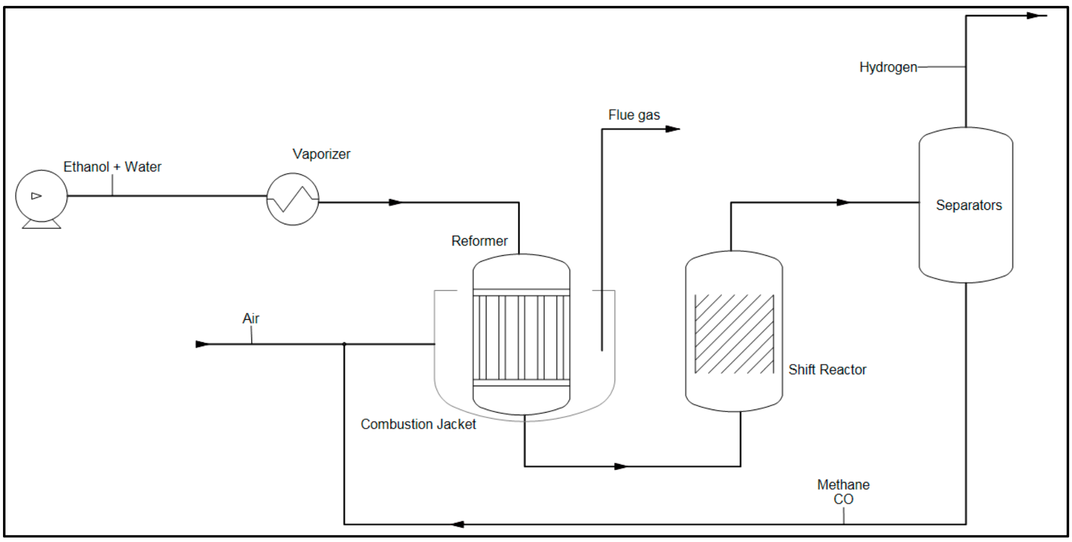

Figure 3. *Cont.*

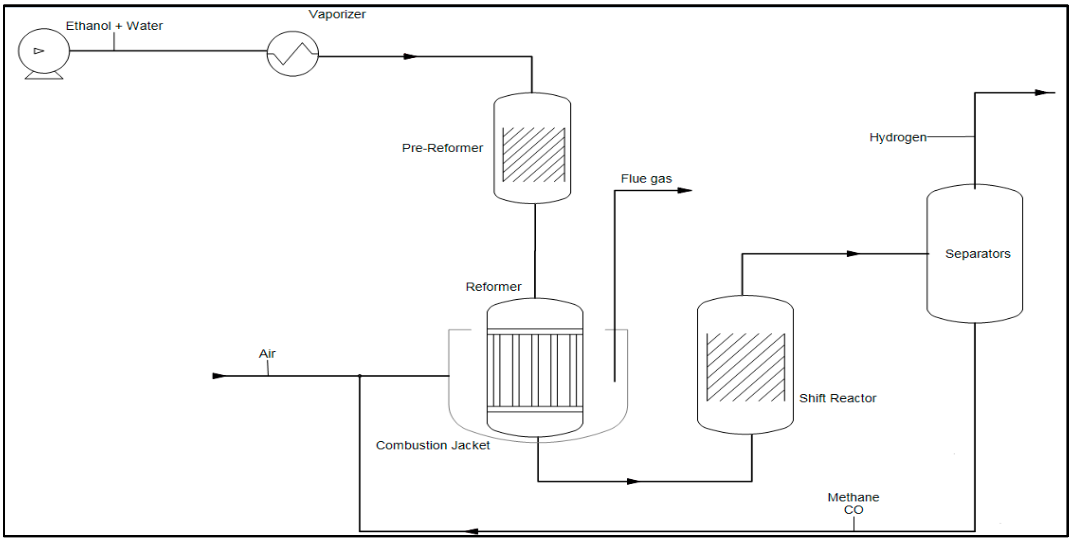

Figure 3. Flowsheet for ethanol steam reforming without (**top**) or with (**bottom**) a separate stage for the two-step conversion of methane, readapted from reference [26].

With these configurations and the typical operating condition specified below, the overall material balances obtained are as follows (Table 2, [26]). These results are obtained on the basis of the thermodynamic 'atom equilibrium', only, and are therefore useful to find the maximum hydrogen yield or to represent reactors with an excess catalyst hold-up.

Table 2. Principal data from [26]. (*) This datum is referred to the overall flowsheet input.

Parameter	Case 1	Case 2
Reformer inlet T (°C)	800	650
Reformer outlet T (°C)	850	920
Pre-reformer outlet T (°C)	-	370
Separator T (°C)	30–35	30–35
Ethanol feed (kmol/h)	854	914
Water to ethanol ratio (mol/mol)	5	5 (*)
Hydrogen to ethanol yield (mol/mol)	5.2	4.9

ESR grants the highest hydrogen output, but requires also the highest energy input to sustain the reaction. While different strategies are possible to burn directly or indirectly an excess of ethanol (stemming from the basic scheme of Figure 3), another option is to add oxygen to the reactants mixture (this is the so-called Autothermal Reforming, ATR, or Partial Oxidation, POX, strategy, depending on the presence or not of water).

The methodology proposed by the cited authors, however, does not foresee to find the oxygen stoichiometric ratio which yields $\Delta_r H = 0$ (ATR), but to optimize the oxygen amount so to keep a hydrogen output as high as possible.

Figure 4 reports an example of equilibrium calculation, using the same software (Aspen Plus with a Gibbs reactor) and keeping the same thermodynamic model to account for the mixture non-ideality, according to the Peng–Robinson equation of state.

Starting from these findings, Khila et al. [27,28] extended the analysis giving up the solid carbon species representing the catalyst coking (which is indeed minimized for steam-to-ethanol ratios higher than 4 and reforming temperatures above 500 °C, but developing full process flow diagrams with separated WGS and methanation sections for the three options (pure SR, POX, and ATR) and analyzing the exergy inputs and outputs (see the cited reference for the details of this thermodynamic potential). Their results are synthetically reported in Table 3.

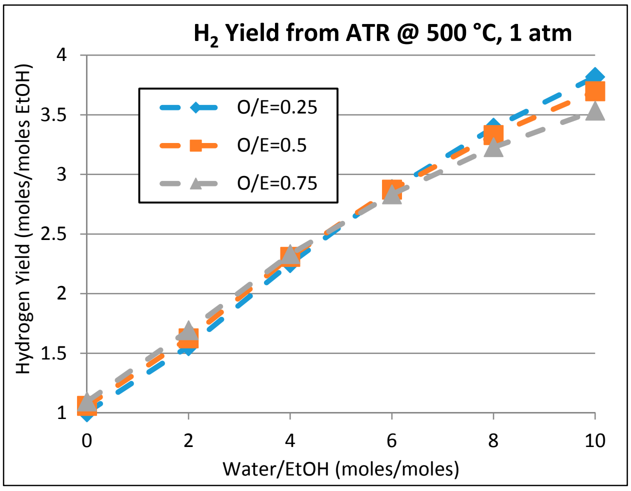

Figure 4. Hydrogen yield (mol/mol of ethanol fed) at equilibrium calculated under the specified conditions. O/E = oxygen/ethanol molar ratio.

Table 3. Selection of data from references [27,28].

Exergy Input (kJ/mol H_2)	407.7	H_2 Yield (mol/mol Ethanol)	3.42
Exergy output (kJ/mol H_2)	295.9	H_2O emission (kg/kg H_2)	14
Electricity input (kJ/kg H_2)	776.6	CO_2 emission (kg/kg H_2)	12
Ethanol feed (kg/kg H_2)	6.73	CO emission (kg/kg H_2)	0.00
Water feed (kg/kg H_2)	15.8	CH_4 emission (kg/kg H_2)	0.032

Besides the value of hydrogen as chemical, its preferred use is perhaps the electric power obtained from the Fuel Cell (FC) systems. The coupling of a reforming plus a FC block allows then to simulate the full 'ethanol-to-electricity' process.

Focusing the attention on the general balances, several works are reviewed which treat essentially the cell as an equilibrium reactor: the hydrogen fed is related to the available power (or voltage/current) via semi-empirical correlations that subtract the expectedly wasted energy, or, equivalently, the potential drop and parasite currents [21,29–31].

Starting from the SR reactions, an integrated analysis of the cell power and heat needs has been performed in [32] using HYSIS® and the flowsheet outlined below (Figure 5), with the main findings reported in Table 4. The details of the heat analysis and its implementation with very specific HYSIS® tools is here omitted and can be found in the cited work. The 1 kW FC is modeled correcting the Faraday relation for ΔE_{rev} with a known relation for the potential drops, while the reformer yields the thermodynamic equilibrium fractions.

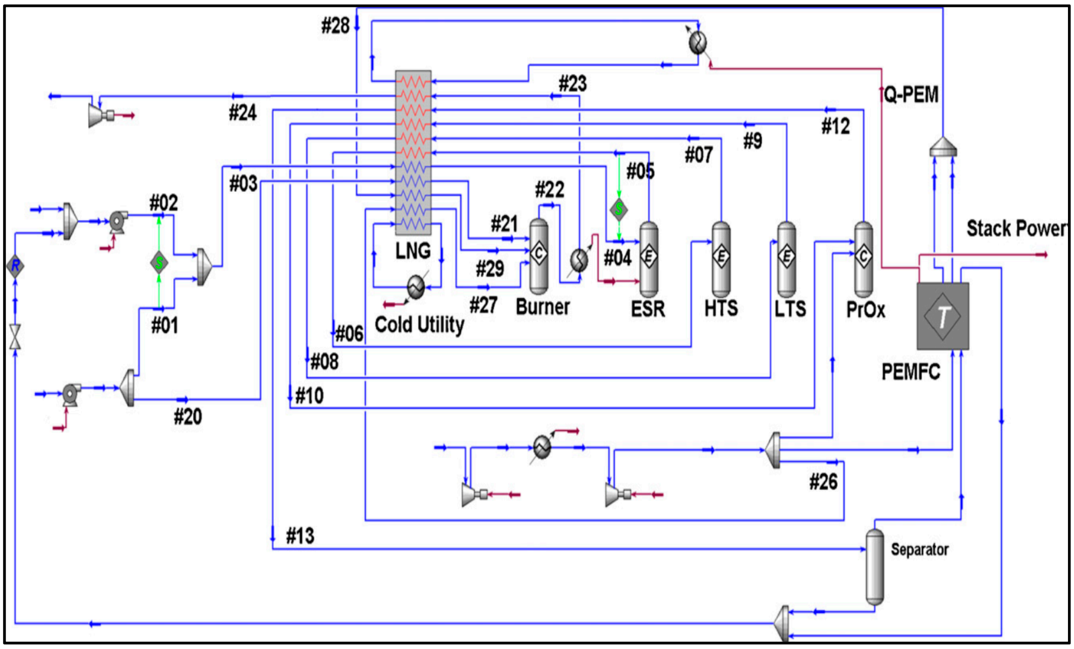

Figure 5. Overall PFD for the ethanol reforming as described in [32]: the pumps are for water (above) to the reformer, fed with fresh water and condensate from the reacted mixture and from the cell, and ethanol (below) to the reformer (after mixing with water) and directly to the burner. Air to the burner, to the byproducts oxidizer ("PrOx") and to the cell is provided by the compressors in the lower middle of the scheme. Notice the special multiple-currents heat exchanger-type block ("LNG"), which is more properly a nested subroutine capable of solving a basic pinch analysis (limited, in this case, to a 20 temperature intervals discretization) of all the cold and hot streams routed through the block. The heat released by the fuel cell is added to the balance of the network via a closed service loop, since the LNG block cannot discharge directly a heat stream on the CU; a HU is not present because the more demanding stream (the already pre-heated reformer feed) is connected to the burner via another heat stream external to the PA block. The image is reproduced by kind permission from [32]. Copyright 2007, Elsevier.

Table 4. Selection of data from reference [32]; the maximum fraction of methane in every stream is always lower than 2.5%.

Material Balances							
Stream	4	5	7	9	12	14	28
T (°C)	709	709	539	237	406	80	80
P (atm)	3	3	3	3	3	3	3
Flow (kmol/h)	0.0367	0.0628	0.0628	0.0628	0.0658	0.0636	0.1749
Fractions							
Ethanol (mol/mol)	0.20	0.00	0.00	0.00	0.00	0.00	0.00
Water (mol/mol)	0.80	0.28	0.24	0.17	0.18	0.15	0.15
Hydrogen (mol/mol)	0.00	0.49	0.52	0.59	0.55	0.57	0.04
CO/CO_2 (mol/mol)	0.00	1.17	0.58	0.03	0.00	0.00	0.00
O_2 (mol/mol)	0.00	0.00	0.00	0.00	0.00	0.00	0.08

Energy Balances					
Parameter	Cold Streams	Cold Utility	Hot Streams	Reformer	Fuel Cell
Lower T (°C)	25–142	20	80–810	709	55
Higher T (°C)	126–709	25	406–1035	709	65
Duty (kW)	1.47	1.07	1.88	0.41	1.06

A conceptually equivalent simulation has been performed by Jaggi et al. [33] with Aspen Plus®, but with manually laying out the heat-exchange network rather than resorting to a built-in software feature. Both the reformer and the FC are modeled based on a known stoichiometry (SR plus WGS and MR for the reactor, hydrogen combustion for the cell with assumed values for the electric and entropic powers in which the enthalpy difference is split). Focusing on the balance between the FC output and the thermal energy recovered by the residual methane and CO burning, these authors define the overall system efficiency as the electric power divided by the enthalpy content of the ethanol fed. Their esteems are reported in Table 5.

Table 5. Data from reference [33] for a FC with the following characteristics: power = 5 kW; nominal stack voltage = 24 V; nominal cell voltage = 0.55 V; cells in stack = 88; current = 208 A; current density = 0.5 A/cm^2; cell area = 406 cm^2.

Parameter	FC T = 200 °C	FC T = 180 °C	FC T = 160 °C
Output ΔV/desired ΔV (V/V)	0.55	0.55	0.55
Current density (A/cm^2)	0.5	0.37	0.2
Current drawn (A)	208	153	83.2
Electric power (kW)	5	3.7	1.99
Overall efficiency	0.45	0.33	0.18

One can notice that both these configurations can be considered as 'autothermal reforming' ones, from a general point of view, since a co-feed of oxygen is actually injected in the burners, giving overall enthalpy balances more favorable than those of the pure SR without necessarily adding fresh fuels to this section—the situation, however, retains a practical difference since the heat exchange network is of course different from the true auto-sustained configuration of a non-endothermic reaction.

These results then define the thermodynamic boundaries of the ethanol reforming process as calculated with the state of the art process simulators.

Moving further, a 'native' ATR process has been calculated by Aicher et al. [34] in a study that combines steady-state simulation, experimental data and dynamic recording of several process variables (the used software is Chemcad). Despite the lab-scale of the study, it is interesting to notice that the used plug-flow reactors can be actually simulated by equilibrium/stoichiometry modules in the proper conditions and catalysts hold-ups. The hydrogen output is quite high (Table 6) and is obtained with a minimal heat-exchange configuration (just the Product-to-Feed auto-exchange is present, plus the combustion), though the authors do not give the full material and heat balances to discriminate between the 'in-reactor' energy saving and the heat released in the other combustions.

Table 6. Data from reference [34] for a process configuration involving a reformer, two WGS stages and one methane post-processor in series (MR). Feeding water/ethanol = 5 mol/mol; feeding oxygen/ethanol = 0.9 mol/mol; reformer inlet = 390 °C.

Unit Output	T (°C) Measured	H_2 (Vol/Vol %)		CO/CO_2 (Vol/Vol %)		CH_4 (Vol/Vol %)	
		Measured	Simulated	Measured	Simulated	Measured	Simulated
ATR reactor	745	37.6	38.8	2.00	1.71	0.13	0.01
WGS stage 1	400	41.5	42.9	19.8	11.5	0.13	0.01
WGS stage 2	290	41.9	43.5	93.18	41	0.13	0.01
MR reactor	220	40.8	42.6	-	-	0.67	0.52

A full integration between a process simulation and a dynamical solution of the time-dependent quantities has recently been performed by Degliuomini et al. [35,36]. The whole system is divided into "fast" sections which can be always considered in equilibrium and are solved by a HYSIS® steady-state simulation (the flow machinery, the equilibrium burner and the heat-exchange network treated with the same tools as in [32]), while the "slow", time dependent, sections that link the equilibrium ones are calculated with MATLAB. All the reactors are treated as plug-flow ones, with full Arrhenius expansions of the reaction rates, and also the mass balances of the FC are treated as transient.

The interested reader may find every computational detail in the given reference. Here, we point out that the whole analysis is meant to control the H_2 flow to the FC, and the foreseen control system handle very well a variation in the electric power requirement, while it cannot avoid some spurious peak in the hydrogen yield in front of a variation of ethanol purity.

The same group further refined the above described control system [35,36], reassessing its validity and comparing the effectiveness of different control strategies (based on different process parameters on which to base the system response) when the integrated reformer/FC system is to be used for automotive purposes.

We complete the analysis considering the other two simulations. The first [37] compares the SR and ATR processes. The calculations were done with ASPEN Plus, with two different heat-integration configurations for both cases, of two different feedstocks, ethanol and bio-diesel (represented mainly as maleiC–Oleate). The gas flow composition at the FC inlet in the selected operating conditions are lumped in Table 7 for an easier comparison.

Table 7. Data extracted from reference [37]. SR performed with reactor outlet at T = 800 °C and feeding water/ethanol = 6 mol/mol; ATR performed with oxygen/ethanol = 0.35 mol/mol and water/ethanol = 4 mol/mol. Methane was always absent.

Process Data	Steam Reforming Fractions (Vol/Vol %)		ATR Fractions (Vol/Vol %)	
Species	**Ethanol**	**Biodiesel**	**Ethanol**	**Biodiesel**
H_2	54.1	56.8	29.6	30.5
H_2O	27.7	22.9	24.3	19.6
CO/CO_2	0.022	0.025	0.013	0.018
N_2	-	-	30.3	32.5

The second case [38], performed with HYSIS®, compares the hydrogen yield obtained from a conventional ehanol steam reformer to the one coming from an electro-chemical reformer (Table 8). Since the data on the operating performance of the two different reactors are found elsewhere (see references addressed in the cited work), the interest of this simulation lies mainly in the fact that the electrical process required a simpler configuration, since the heat-exchange network and the pre-heating were not needed.

Table 8. Data extracted from reference [38].

Parameter	Steam Reforming	Electrical Reforming
Hydrogen Yield (kg/kg EtOH)	0.03	0.044
Overall Energy Input (kWh/kg H_2)	33	28

From the above reported examples, the need to properly predict the behavior of the different reactors underlines the requirement of complete and reliable kinetic models as the basis for this simulation activity. This point will be addressed in the following sections.

2.2. Kinetic and Theoretical Analysis of Ethanol Reforming

The analysis of catalytic ethanol reforming implies essentially three steps: (1) the selection of the conditions, for each catalyst, to obtain high conversion and a good selectivity; (2) the comparison of the reforming products mixture with the one expected at thermodynamic equilibrium; (3) the rationalization of these data in terms of a chosen mechanism.

The first step involves mainly a catalyst synthesis, characterization and activity testing: statistical procedures help indeed in the eventual interpretation of data [25], but at this stage the most important goal is the correlation of a products yield to the relevant catalyst features, or the comparison between different catalysts: as an example of this kind of analysis, see the various species yields on different materials as tested in [39].

At the second step, the catalyst selectivity towards a whole reaction path rather than towards a product becomes clearer. In fact, since equilibrium conditions depend on the temperature (most of the test reactors works with negligible pressure drops), when the full conversion of the precursor is achieved then the possible byproducts reveal that a certain path is kinetically forbidden (or enhanced), and if the ratios of H_2O, CO, CO_2, H_2, and CH_4 differ from the thermodynamically expected ones then even equilibrating reactions are kinetically delayed. Therefore, the study of reforming mixtures as a function of the reaction temperature can show if a material is always active towards any reaction path until the ultimate equilibrium or, on the other side, if the activation barriers between each reaction are appreciably different (for this kind of analysis, see for example the above cited papers and [40–42]).

The third step can be performed essentially in two ways: (i) a mechanism is postulated according to the intermediates, then the relative reaction rates are extrapolated evaluating the amount of products as a function of the contact time (which, at this stage, becomes the most important parameter), then the variation of the temperature allows the extrapolation of the activation energies; (ii) the interaction between reactants and catalyst is studied a priori relying only on the quantum mechanical models of the interacting atoms: virtually any possible bond break and formation (or a wide selection of them) is tested and the corresponding elementary reaction rate is quantified (via the Eyring model) until all the steps from reactants to products are linked.

2.2.1. ESR: Conversion Rates and Steady States

As shown by equilibrium calculations (for example, [43,44], for two different methodologies) a sufficient loading of a catalyst with the correct selectivity towards the reforming can eliminate any byproduct (except methane) when working at the proper temperature.

In this context, the simplest kinetic model that can be formulated on the stoichiometric ground is as follows:

$$\mathrm{EtOH} + \mathrm{H_2O} \xrightarrow{\mathrm{k_r}} \mathrm{CH_4} + \mathrm{CO_2} + 2\mathrm{H_2} \tag{R3}$$

$$\mathrm{CH_4} + \mathrm{H_2O} \rightleftharpoons \mathrm{CO} + 3\mathrm{H_2} \tag{R4}$$

$$\mathrm{CO} + \mathrm{H_2O} \rightleftharpoons \mathrm{CO_2} + \mathrm{H_2} \tag{R5}$$

In order to quantify just the conversion rate of ethanol, mass-transfer steps (i.e., how the species diffuse through the material pores and within the gaseous stream) are typically not relevant for the reaction. The equilibrium reactions, in turn, do not affect ethanol conversion if this is truly not-reversible (tests performed in plug-flow reactors actually divide ethanol conversion and equilibration also spatially). If, moreover, the water to ethanol ratio is sufficiently high and the reactants are diluted in an excess of inert carrier, then the model can be reduced to a pseudo-homogenous first-order one:

$$\frac{dp_{EtOH}}{d\tau} = -k_r\, p_{EtOH} \text{ with } k_r = k_r^0 \exp\left(-\frac{E_a}{RT}\right) \tag{7}$$

where τ represents the contact time, i.e., the time for the given volumetric flowrate of the reaction mixture to travel across the catalytic volume.

If the water to ethanol ratio in the mixture is not high enough and the first-order simplification has to be dropped, the next step is to resort to an empirical general formulation based on kinetic pseudo-orders:

$$\frac{dp_{EtOH}}{d\tau} = -k_r\, p_{EtOH}^a\, {p_{H_2O}}^b \tag{8}$$

This kind of analysis is used in [45–47], where catalysts of Ru/Al_2O_3, $Ni/MgO/Al_2O$ and Ni/Al_2O_3 yielded the following kinetic parameters (Table 9). Notice very small values of the activation energy, which may indicate the presence of diffusional limitations or of highly correlated parameters.

Moving further and considering that the outcome of this conversion is a mixture of four species, the amounts of CH_4, CO, CO_2, and H_2 can provide an idea of the kinetic importance of the equilibria with respect to the conversion. For example, the study performed in [48] reported the following outcome (Table 10) on the state of methanation reaction over a Rh catalyst supported on Ceria-Zirconia.

Table 9. Data as from Table 2 of reference [45], Equation (6) of reference [46] and Table 4 of reference [47]. The values for k_r^0 and E_a from reference [45] (not reported in the same form, but as calculated constants at different temperatures) have been fitted with Excel™ REGRLIN (r^2 = 0.9446), while the power-law model of reference [32] was originally presented in terms of molar flowrates rather than partial pressures.

Catalyst	k_r^0	E_a	a	b
Reference [45] (Ru/alumina)	55,881 ($cm^3\ g_{cat}{}^{-1}\ h^{-1}$)	42 (kJ/mol)	1	0
Reference [46] ($Ni/MgO/Al_2O$)	439 ($mol\ min^{-1}\ g_{cat}{}^{-1}\ atm^{-3.42}$)	23 (kJ/mol)	0.711	2.71
Reference [47] (Ni/alumina)	0.031 ($mol\ g_{cat}{}^{-1}\ s^{-1}$)	4.41 (kJ/mol)	0.43	0

Table 10. Data extracted from Table 5 of reference [48]. The yield of different products with respect to the ethanol fed (and of residual water among the reactants) is reported as measured outflowing value, to be compared with that calculated at equilibrium at the same temperature.

Temperature (°C)	500		550		600	
Yield (mol/mol Ethanol)	**Measured**	**Equilibrium**	**Measured**	**Equilibrium**	**Measured**	**Equilibrium**
H_2O	4.00	2.99	4.00	2.68	2.36	2.41
H_2	1.56	2.15	1.85	2.96	3.63	3.78
CO/CO_2	0.64	0.25	0.61	0.32	0.48	0.62
CH_4	0.21	0.93	0.28	0.68	0.50	0.39
C_2H_4	0.025	0.000	0.015	0.000	0.000	0.000

In the same work, the activity of the catalyst towards the WGS reaction was tested, showing values nearer to the equilibrium ones, but only in certain temperature ranges and with a dependency on the feed composition. Therefore, the authors concluded that, even if no intermediate conversion products 'survive', their production/conversion rates are comparable with the rates of the 'lumped' ethanol conversion and of the equilibration steps, and that the mechanism leading to methane (and from it to CO and CO_2) depends on the catalyst.

2.2.2. ESR: From Stoichiometry to Mechanism

The first way to account for the reforming mechanism even when, on experimental ground, only ethanol conversion is measured and byproducts are absent, is to verify the true rate determining step (RDS) between the three above reactions. This approach was followed by Akande et al. [47], who further divided the ethanol splitting reaction into two steps (ethanol adsorption and the actual C–C break) and lumped methanation and WGS reactions into one stoichiometry but allowing for two different paths (* represent a surface active site):

$$C_2H_6O + * \rightleftarrows C_2H_6O^* \tag{R6}$$

$$C_2H_6O^* + * \rightleftarrows CH_4O^* + CH_2^* \tag{R7}$$

$$CH_4O^* + H_2O \rightleftarrows CO_2 + 3\,H_2 + * \tag{R8}$$

$$CH_2^* + 2\,H_2O \rightarrow CO_2 + 3\,H_2 + * \tag{R9}$$

Barring the detail, and noticing that this work does not account for CO in the mixture or on the catalyst (Ni/Al_2O_3), we point out that even this simple analysis yielded comparable activation energies and mean square errors (MSE, we mean calculated concentrations versus measured ones, for the best extrapolated values of the kinetic parameters) when the RDS was considered the second or the third, confirming on a purely kinetic ground that the methanation and WGS reactions may not be faster than the C–C break and sensitive to the mechanism being actually followed (Table 11).

Table 11. Data taken from Table 4 of reference [47], prefactors of the kinetic constants are not reported, since the different tested mechanism lead to a difference in the reaction orders and then in the measuring units. The MSE (Mean Square Error) is reported by the authors as the absolute value of the deviation between predicted and observed conversion rates, normalized to the observed rate.

RDS	E_a (J/mol)	MSE
2	4430	6.0%
3	3550	10.6%

Only by considering qualitative data obtained below 100% conversion it is possible to discriminate another RDS even prior to C–C break, for example the formation of acetaldehyde as the main path for oxidative ethanol reforming (for example [49,50] among others), even when this chemical is not recognized in the product mixture thanks to the catalyst loading or other reaction conditions that favor its fast conversion into methane. A simple, yet straightforward, step in this direction is the work by Wang et al. [51], who maintained the basic stoichiometry already described with another set of four elementary steps:

$$C_2H_5OH^* + H_2O^* + * \rightarrow 2\,CO + 4\,H_2 + * + * + * \tag{R10}$$

$$C_2H_5OH^* + * + * \rightarrow C_2H_5O^* + H_2 + * + * \tag{R11}$$

$$C_2H_5O^* + * \rightarrow CH_4 + CO + * + * \tag{R12}$$

$$CO^* + H_2O^* + * \leftrightarrows CO_2{}^* + H_2 + * + * \tag{R13}$$

Contextually, the same authors showed (thanks to a collection of data taken on an Ir/CeO_2 catalyst with a variable amount of any species in the feed stream) that a simple power law model based on pseudo-kinetic orders may not be accurate enough and the catalyst surface covering has to be addressed at least in a heuristic way. The interested reader can further investigate this point with the help of the data contained in Figures 4–7 of the above mentioned work and of the synthetic review of several power-law models (Table 2, ibidem). Here we just notice that, despite the simplicity of the proposed mechanism—basically, a stoichiometry for the path: ethanol $\rightarrow$ acetaldehyde $\rightarrow$ methane—the addition of a further kinetically relevant stage actually improves the description of the reforming process, and the choice to separate the adsorbed species into two different adsorption sites is consistent with the recognized importance of the support material beside the active metal. At a glance, the main findings of this work are reported in Table 12.

Table 12. Data taken from reference [51] (see also references therein) for the rates of the above rate determining steps (RDS) and for the adsorption equilibria of the relevant species on the catalyst: the constants are calculated at 818 K and the tolerances at the 95% confidence level.

RDS	K (mol $kg_{cat}{}^{-1}$ s^{-1})	E_a (kJ/mol)	Species	K (kPa^{-1})	ΔH (kJ/mol)
1	11 ± 1	85 ± 14	ethanol	25	n.a.
2	9 ± 0.01	32 ± 15	water	3×10^{-4}	−55
3	23 ± 5	66 ± 29	CO_2	2×10^{-3}	−67
4	20	109 ± 19	CO	1	−80
			H_2	0.01	−110

In parallel, Mas and coworkers [52] developed the reforming mechanism considering the production of methane, giving less importance to the aldehyde as a kinetically relevant intermediate, but helping to establish the methanation reaction as a RDS itself (rather than a fast equilibrium stage), accounting for the different behavior of this species on different catalysts.

The same authors substantially refined the first proposed kinetic model in a later work [53], based on an extensive data collection obtained by tests on a catalysts of Ni/alumina and Ni(II)/Al(III), taking advantage of the mechanism selection already worked out by Graschinsky et al. [54] (data from a Rh/magnesia/alumina catalyst) and of a similar work by Sahoo et al. [55] to explain their own data (Co/alumina). While these papers share the same core of RDS, the latter authors adopt an abridged stoichiometry where the methanation is not treated explicitly, as it were just the 'equilibration link' between "dry reforming" and a full "steam reforming". In any case, acetaldehyde is considered as the key intermediate, even if rapidly converted before its possible desorption, via a sequence of steps such as:

$$C_2H_5OH^* + 2* \rightleftarrows C_2H_4O^* + 2\,H^* \tag{R14}$$

$$C_2H_4O^* + * \rightleftarrows CH_3{}^* + CHO^* \tag{R15}$$

$$CH\,{}^* + 2\,OH^* \rightleftarrows CO_2{}^* + H_2^* + H^* \tag{R16}$$

$$CHO\,{}^* + OH^* \rightarrow CO_2{}^* + H_2^* \tag{R17}$$

$$CO_2{}^* + H^* \rightleftarrows CO^* + OH^* \tag{R18}$$

These works provide a body of kinetic and thermodynamic parameters that constitute the starting point for LHHW kinetics bridging elementary reaction steps to the fitted experimental data, in conditions where byproducts and coking can be neglected. A brief selection of values is outlined in Table 13 for the following common stoichiometry:

$$C_2H_5OH + H_2O \rightarrow 2H_2 + CO_2 + CH_4 \tag{R19}$$

$$C_2H_5OH \rightarrow CO + CH_4 + H_2 \tag{R20}$$

$$C_2H_5OH + 3H_2O \rightarrow 6H_2 + 2CO_2 \tag{R21}$$

$$CO + H_2O \rightleftarrows CO_2 + H_2 \tag{R22}$$

Table 13. Data from reference [52,55]. (*) this reaction is found written in the inverse sense; (**) the original paper reports likely mistyped units: the values are useful only for a comparison of the relative values.

Reference	[52]	[53]	[54]	[55]
Cat	Ni/ Alumina	Ni(II)/Al(III)	$Rh/MgAl_2O_4/Al_2O_3$	Co/Al_2O_3
*K*1	-	3.06×10^{-7} (mol mgcat^{-1} min^{-1})	-	-
*K*2	-	1.13×10^{-7} (mol mgcat^{-1} min^{-1})	-	4.46×10^{19} (m^2 mol^{-1} s^{-1}) (**)
*K*3	-	-	-	1.16×10^{20} (m^2 mol^{-1} s^{-1}) (**)
*K*4	-	9.12×10^{-4} (mol mgcat^{-1} min^{-1}) (*)	-	4.64×10^{16} (m^2 mol^{-1} s^{-1}) (**)
E_a1	235.06 (kJ/mol)	195.5 (kJ/mol)	418 (kJ/mol)	-
E_a2	278.74 (kJ/mol)	122.9 (kJ/mol)	85.9 (kJ/mol)	71.3 (kJ/mol)
E_a3	-	-	-	82.7 (kJ/mol)
E_a4	-	166.3 (kJ/mol) (*)	107 (kJ/mol)	43.6 (kJ/mol)

2.2.3. Other Reforming Models

All the above cited models, though developing the reaction pattern yielding all the equilibrium reforming products, rely on data collected with reactors that can be treated by the ideal isothermal, isobaric PLUG-FLOW model, with neither any axial back-diffusion of the chemicals nor any mass transfer limitations. The correct modeling of these latter kinetics requires the implementation of PDE systems for every mass transport mechanism and possible heat transfers, if the foreseen system requires it. Without going into the details of this wider research field, we briefly account for at least three interesting aspects: (i) the intrinsic mass and heat transfer limitations of wall-coated microchannel reactors [56–58]; (ii) the time on stream-dependent kinetics due to the (relatively) slow and selective adsorption/release of a species [59,60]; (iii) the former phenomenon described in non-ideal reactors characterized by temperature as well as pressure gradients [61,62].

We conclude this section on the experimental kinetics addressing also a couple of studies on the oxidative reforming of ethanol. The qualitative catalyst comparison by Fierro et al. [63] showed the importance of the catalyst support along with the prevailing kinetic character of the reaction. The detailed theoretical and experimental work of Mondal et al. [64], where two mechanisms proceeding via acetaldehyde scission and the production of formic acid/formiates are compared and complemented by an interesting statistical analysis of the model parameters and the testing reaction outputs.

2.2.4. ESR: From Chemical Bonds to Hydrogen

Increasingly complex reaction mechanisms and thus kinetic models may result in very complex kinetic testing. This is needed to provide sufficient experimental data to account for increasing number of parameters to be fitted. Nevertheless, complex kinetic models may end in strongly correlated kinetic parameters, which at the end may lose reliability.

Reverting the perspective, it is nowadays possible to look at the reaction mechanism at the atomic level and just ab initio (without any prior selection of intermediates to be found), thanks to the increased availability and reliability of computational algorithms based on a first-principle quantum mechanic approach. All the works reviewed here resort to a specific electronic structure method called Density Functional Theory to estimate the interaction energy between atoms while taking into account the composition of the catalytic materials and the arrangements of the atoms in the solid. In principle, this approach may support kinetic modelling, providing independent kinetic or thermodynamic parameters, thereby limiting the number of parameters to be estimated by regression of kinetic data, hence the correlation between parameters.

Considering an ethanol molecule interacting with a solid, a straightforward pre-selection of the relevant bond-ruptures allows to concentrate on the C atom linked to the oxygen, giving four possible initial routes for the decomposition (Figure 6).

CH_3–CH–OH + H ↖ ↗ CH_3–CH–OH + H

$CH_3 - CH_2 - OH$

CH_3 + –CH_2–OH ↙ ↘ CH_3–CH_2– + OH

Figure 6. The four bond breaking options relative to the C atom linked to the oxygen. It represents the starting point in many analyses on ethanol degradation. The top two paths are considered distinct.

The route to each possible product across the potential energy surface is then explored to find the lowest-energy barrier to overcome, so that the activation energy and heat of reaction can be determined for each elementary step. With this approach, Wang et al. [65] compared the relative energy barriers for the above mentioned initial paths on a whole set of noble metals. The analysis was also repeated for these dissociation paths to take place after the initial dehydrogenation EtOH $\rightarrow$ EtO^-. Without reporting all the data, one of the more probable reaction mechanisms is shown below, as asserted for Rh and Ni (1,1,1) crystalline plane (Table 14 and Figure 7).

Table 14. Data from reference [65], showing the energetic barriers (number on the left of the second and third column) and heats of reaction (number on the right) (eV) of the indicated elementary steps, selected as the favorite ones.

Step	Rh	Ni
(1) $C_2H_5OH* \rightarrow C*H_2CH_2OH* + H*$	0.52/0.45	1.46/0.51
(2) $C*H_2CH_2OH* \rightarrow C*H_2C*H_2 + HO* + H*$	0.42/−0.69	0.14/−0.73
(3) $C*H_2C*H_2 + HO* + H* \rightarrow 2\,H_2C* + HO* + H*$	0.99/0.82	1.04/1.02
(4) $C_2H_5O* \rightarrow C*H_2CH_2O* + H*$	0.55/0.52	1.57/1.15
(5) $C_2H_5O* \rightarrow C*H_2C*H_2 + O* + H*$	0.05/−1.10	0.10/−1.33
(6) $C*H_2C*H_2 + O* + H* \rightarrow 2\,H_2C* + O* + H*$	0.97/0.84	1.05/1.01

In this paper, the interested reader also finds a correlation between the activation energies of these transitions and an energetic parameter representative of these d-transition metals, what is known as *d*-band model [66].

A similar analysis was performed later by Sutton and Vlachos [67], who tried to correlate the preferred reaction paths on six transition metals to their ethanol-binding ability, rather than on more general lattice properties: the authors established a link between the M-O binding energy and several critical bond-ruptures (e.g., C–C, C–O), while a comparison between the modeled metals can be appreciated at a glance in Figure 8.

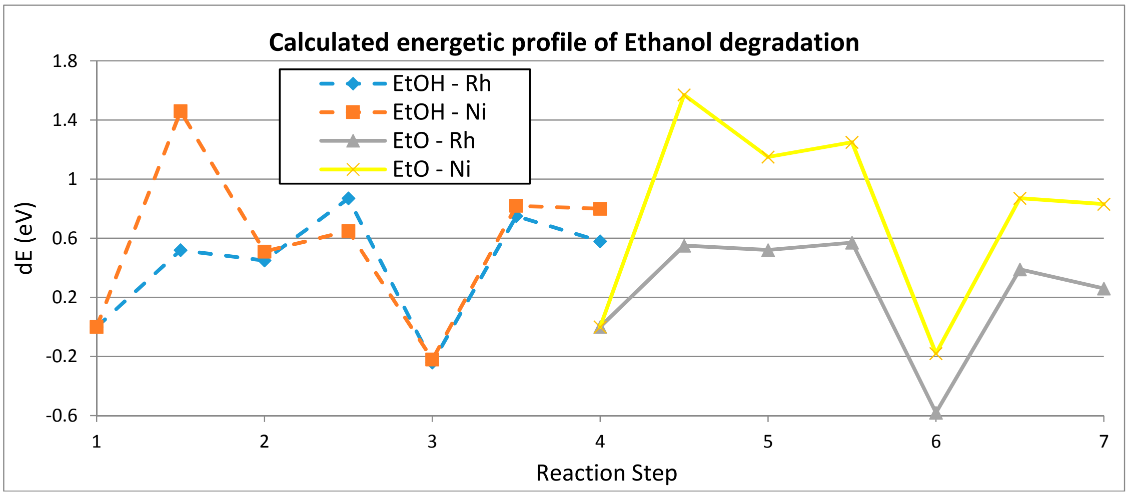

Figure 7. Graphic representation of the elementary reaction steps relative to Table 14; the initial adsorbate is conventionally placed at the 'zero' energy level.

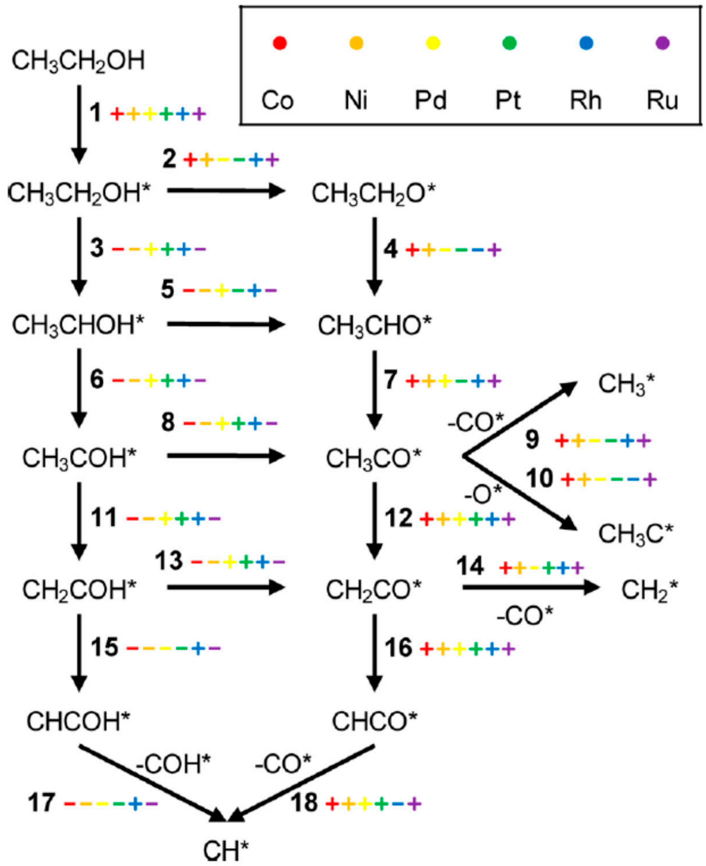

Figure 8. Sketched preferential paths on six noble metals as outlined in reference [67]. Reproduced from [67]). Copyright 2015, ACS.

The same authors focused later on platinum [68], performing an extensive analysis of all of the possible bond-breakings from ethanol down to carbon monoxide together with the reversible de-hydrogenations linking methane to the CH_x groups. This comprehensive study is complemented by the fit of a set of conversion data, obtained adjusting just a scale-normalization factor. Importantly, this first-principle analysis confirms the kinetic relevance of the H-abstraction steps that lead to acetaldehyde formation, postponing the C–C breaking stage, and the eventual re-equilibration of the fragments as precursors of CO, CO_2, and methane (Figure 9).

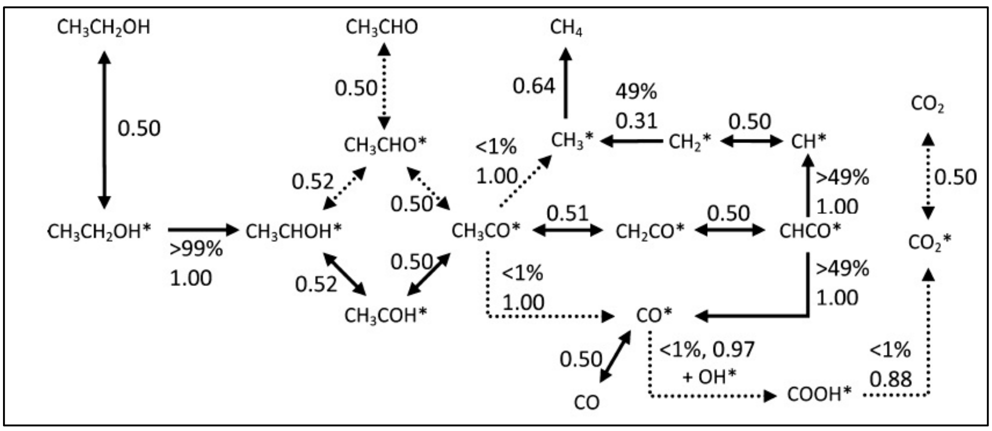

Figure 9. Synthetic scheme of the reforming mechanism, adapted with permission from reference [68]. Copyright 2013, ACS.

A similarly comprehensive mechanism on platinum was developed by Koehle et al. [69] for ethanol partial oxidation, where the total amount of reaction steps (50, each one considered in principle as reversible) was treated with a less aprioristic approach. The activation energy of every bond-break was estimated with a semi-empirical model, the so-called UBI-QEP, that relies on the interpolation of the calculated (or measured) binding energies of the intermediates with two parameters, catalyst coverage, and temperature, that are in turn eventually used to extrapolate the activation energies separating an intermediate from to the other.

Though less rigorous from the theoretical point of view, this work also presents the fit of another set of reforming data, obtained by adjusting less than 10 (out of possible 100) of the already calculated pre-exponential factors. Interestingly, the adjusted reaction steps were chosen via a statistical sensitivity analysis, which points out methane formation and CO oxidation as crucial for the product distribution in the mixture.

2.3. Ethanol to Ethylene

2.3.1. Ethanol to Ethylene: Direct Dehydration

The conversion of ethanol to ethylene is catalyzed by acidic catalyst functions, often attributed to Lewis type sites. It may be the desired reaction for the production of this building block from a renewable source, or it may represent a reaction path parallel to the oxidative one, leading to acetaldehyde and then to carbon–carbon scission and conversion into hydrogen/syngas [70]. In this sense, it is an undesired path because it lowers the H_2 yield, and it is connected with catalyst deactivation by coking. In any case, its kinetics should be detailed in order to perform process simulation or to cope with selectivity/durability issues. Also for this application, first principle methods may help addressing possibly complex reaction pathways.

Experimental results, however, most often provide a more complicated picture. The reasons are that (i) most of the used catalysts are actually bifunctional (with a transition metal active towards the C–H bond activation and a more or less acidic support oxide) and (ii) depending on temperature, both acetaldehyde and ethylene can be reversibly converted into CO and methane. Putting aside at first instance the selectivity matter, it is possible to start the energetic analysis of the ethanol-to-ethylene path by itself: then a comparison of the elementary steps on different catalysts can explain their selectivity 'a posteriori', analyzing those points whence expected byproducts or alternative routes stem. Following this approach, a very straightforward yet indicative DFT calculation of the dehydration in differently doped Zeolites was performed in [71] (Table 15).

Table 15. Data from reference [7] for the reactions: $^{(a)}$ EtOH* $\rightarrow$ [TS‡] and $^{(b)}$ EtOH $\rightarrow$ C_2H_4 + H_2O.

Catalyst	H–ZSM–5	Cu–ZSM–5	Ag–ZSM–5	Au–ZSM–5
$\Delta G^{\ddagger(a)}$ kcal/mol	43.86	52.75	40.1	36.29
$\Delta G^{(b)}$ kcal/mol	4.76	4.76	4.76	4.76

The choice of just one reaction path for every catalyst with the C–O bond progressively loosing may be somehow simplified, but it establishes a direct link between theoretical calculations and the well-known empiric concept of a "functional group", still applicable with catalysts and conditions, which yield a 100% selectivity.

Moving a step further, Kim et al. [72] extended the a priori study of the dehydration in two directions, even if focusing on the H-ZSM-5 catalyst, only: a comparison between two different mechanisms and a benchmark of different computational strategies. We report here a synopsis of the main findings (Table 16 and Figure 10); the reader can check out the computational and mechanistic details in the cited reference with its supporting material.

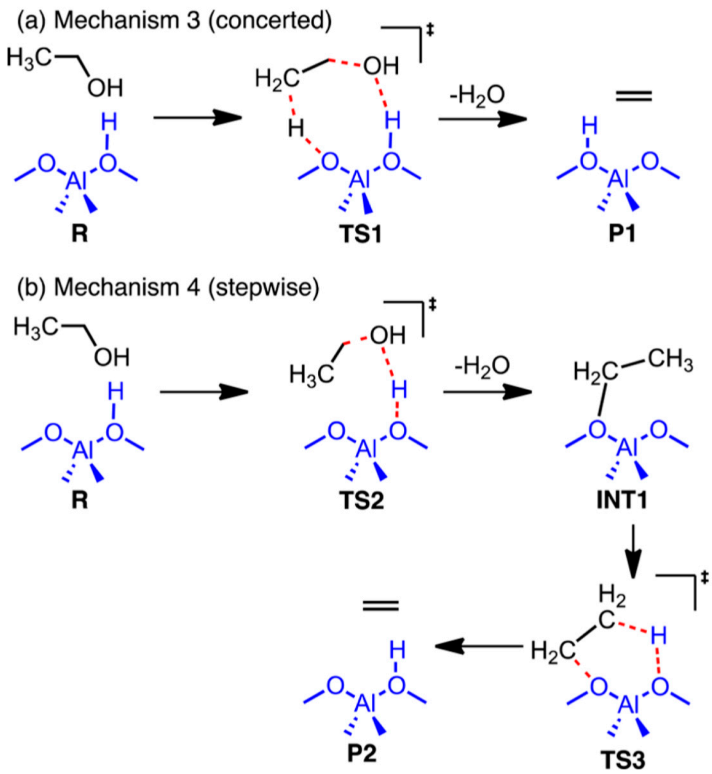

Figure 10. Schemes of the mechanisms studied in for ethanol dehydration on a zeolite catalyst [72]. Reproduced from [72]. Copyright 2015, ACS. (‡ denotes an activated intermediate).

Table 16. Data from reference [72]. The reference zero-energy is the lowest of the binding energies of adsorbed ethanol on one of the four O-atoms available at each site: since any of the two mechanisms can then yield different energetic profiles (according to the different O atoms possibly involved), the reported values are the averages, for a given TS, over all these possibilities.

Transition States	Computational Method 1		Computational Method 2	
Intermediate	ΔE	ΔG	ΔE	ΔG
TS 1 (mechanism 3)	50.2 ± 4.2	46.2 ± 4.0	50.2 ± 3.3	46.0 ± 3.3
TS 2 (mechanism 4)	54.3 ± 7.0	51.7 ± 6.7	54.9 ± 2.9	52.2 ± 3.3
TS 3 (mechanism 4)	53.7 ± 5.7	49.5 ± 5.7	51.0 ± 5.0	46.9 ± 4.8

A similar study was performed by Maihom et al. [73] for an iron-doped zeolite (Fe-ZSM-5), analyzing the steric and energetic features of two mechanisms (Figure 11), a step-wise (where ethanol interacts with one catalyst atom at a time) and a concerted one (where ethanol interact simultaneously with two catalyst atoms).

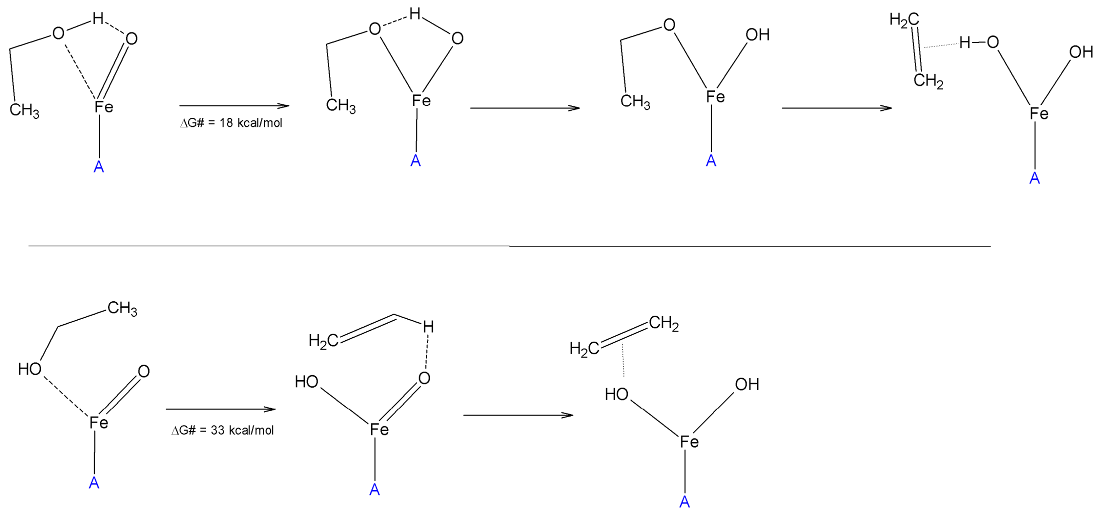

Figure 11. Schematic summary of the mechanisms proposed in reference, readapted from [73].

Qualitatively, it is interesting to note that the mechanism with the higher energetic barriers is not completely excluded, because it shows the lowest barrier for the initial step—moreover, the 'choice' between the two paths depends strongly on the orientation of the alcohol inside the adsorption site.

2.3.2. Ethanol to Ethylene: Parallel Paths

Though only incidentally, in the above works the possibility that –H atom transfer takes place via a bimolecular reaction with a nearby ethanol molecule rather than with the catalyst is also addressed, instrumental to ethylene formation. This phenomenon is related to a possible byproduct of the reaction, i.e., the di-ethyl ether (DEE).

Christiansen et al. [74] studied the reaction of ethanol on γ-alumina theoretically, assigning ethylene formation to an unimolecular mechanism (either step-wise or direct), and further explaining how a bimolecular mechanism may also yield ethylene, but will more likely turn ethanol into DEE (Table 17). Moreover, comparing the reaction rates predicted by the model with a set of experimental data, these authors were able to discard less relevant reaction paths still fitting the observations with a minor adjusting of the already calculated parameters. The inferred mechanism and basic stoichiometry are sketched in Figure 12.

Table 17. Most important elementary steps of the mechanism explained in [74], with the free energies of the intermediates compared to gas-phase values (all numbers in kcal/mol, for T = 488 K). Superscripts 'Al' and 'O' denotes catalysts active atoms.

Elementary Step	$\Delta_r G^0$	$\Delta G^{\ddagger}$ (Calculation)	$\Delta G^{\ddagger}$ (Adjusted)
$CH_3CH_2OH^{Al} + ^{O} \rightleftarrows CH_3CH_2O^{Al} + H^{O}$	−12	2	2
$CH_3CH_2O^{Al} + CH_3CH_2OH^{Al} \rightleftarrows CH_3CH_2OCH_2CH_3Al + OH^{Al}$	−7	28	24
$CH_3CH_2OH^{O} + CH_3CH_2OH^{Al} \rightleftarrows CH_3CH_2OCH_2CH_3 + OH^{Al} + H^{O}$	−16	21	17
$CH_3CH_2OH^{Al} + ^{O} \rightleftarrows C_2H_4 + OH^{Al} + H^{O}$	−16	25	29
$CH_3CH_2O^{Al} \rightleftarrows C_2H_4 + OH^{Al}$	−4	58	58
$CH_3CH_2OCH_2CH_3Al + ^{O} \rightleftarrows C_2H_4 + CH_3CH_2O^{Al} + H^{O}$	−9	29	29

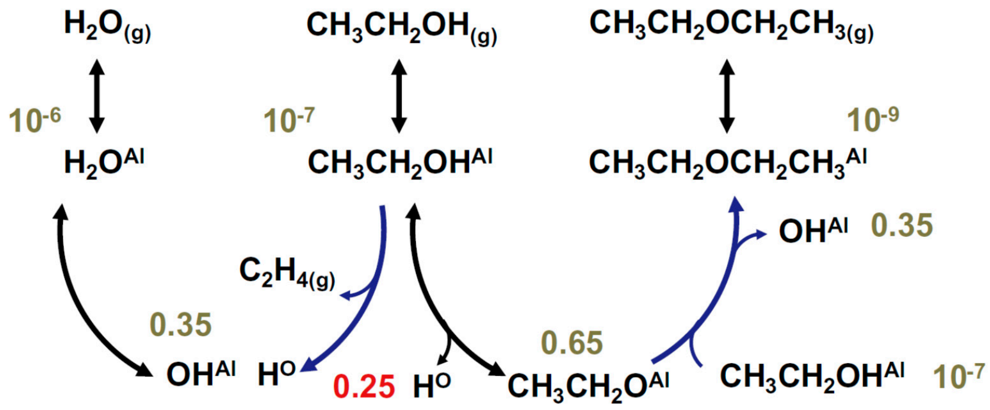

Figure 12. Paths for ethanol conversion to DEE and ethylene [74]. Reproduced from [74]. Copyright 2015, Elsevier.

$$CH_3CH_2OH + {}^{Al} \rightleftharpoons CH_3CH_2OH^{Al} \tag{R23}$$

$$H_2O + {}^{Al} \rightleftharpoons H_2O^{Al} \tag{R24}$$

$$CH_3CH_2OH^{Al} + {}^{O} \rightleftharpoons CH_3CH_2O^{Al} + H^{O} \tag{R25}$$

$$H_2O^{Al} + {}^{O} \rightleftharpoons OH^{Al} + H^{O} \tag{R26}$$

$$CH_3CH_2OH^{Al} + {}^{O} \rightarrow C_2H_4 + OH^{Al} + H^{O} \tag{R27}$$

$$CH_3CH_2OH^{Al} + CH_3CH_2O^{Al} \rightarrow CH_3CH_2OCH_2CH_3 + OH^{Al} \tag{R28}$$

where the superscript Al denotes a surface unsaturated Al site. An extended representation of the process was outlined by Alexopoulos et al. [75] for the already mentioned zeolite HZSM5: the parallel ethylene/DEE figure is modified into a three-fold macro-scheme (Figure 13), where the paths A, B, and C represent in turn a succession of simultaneous and competing elementary steps.

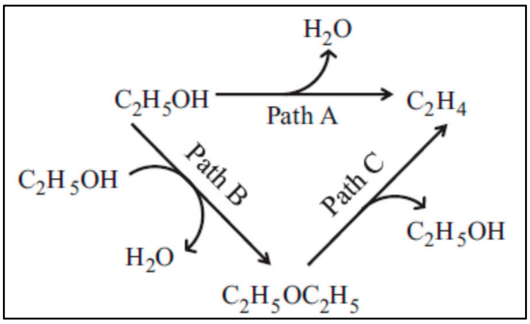

Figure 13. Competing reaction routes as described in reference [75]. Reproduced from [75]. Copyright 2016, Elsevier.

These authors consider again only the catalyst oxygen atoms as directly involved in the bond activation process, however their extended reaction network was able to reproduce a set of contextually collected data without further adjusting the parameters. The relative weight of the possibly competing routes leading to each experimentally observed product was evaluated by a statistical analysis of the calculated reaction rates. Moreover, the authors considered ethanol absorption more important than water in determining the selectivity and the change of mechanism during the conversion. For a more specific comparison, we report the results obtained for the most probable routes to ethylene [A/1-2-3-4-5] and DEE [B/1-6-7-8-9] as extracted from the above-cited paper [75] (Table 18).

Table 18. Data from reference [75]: any step being reversible, equilibrium constants are always calculated via the Eyring model, while E_a and *A* refer to the Arrhenius formulation, and are defined only for rate determining steps (RDS). These, in turn, are selected by the authors on the basis of a statistical screening of the K_{eq} values over a larger range of temperatures and catalyst coverage. Single H* and O* denote active atoms present on the alumina after moisture adsorption. A is given in (s^{-1}) or (10^{-2} kPa^{-1} s^{-1}) for RDS or adsorptions, while K_{eq} is reported in: (10^{-2} kPa^{-1}), (10^2 kPa) or dimensionless for adsorption, desorption, or reactions at the surface, respectively.

	Elementary Step	E_a (kJ/mol)	A	K_{eq} @ 500 K	Notes
(1)	$EtOH + 2* \rightleftarrows EtO^*H^*$	-	-	1.1×10^4	equilibrium
(2)	$EtO^*H^* \leftrightarrows EtO^*H + *$	-	-	8.0×10^{-2}	equilibrium
(3)	$EtO^*H + H^* + O^* \rightleftarrows EtO^* + H_2O$	118	4.0×10^{13}	3.8×10^{-1}	RDS
(4)	$EtO^* \rightleftarrows C_2H_4^* + O^* + H^*$	106	9.4×10^{12}	3.5×10^{-2}	RDS
(5)	$C_2H_4^* \leftrightarrows C_2H_4$	-	-	1.4	equilibrium
(6)	$EtO^*H^* + EtOH \rightleftarrows EtO(H^*) - H - O^*Et$	-	-	7.6×10	equilibrium
(7)	$EtO(H^*) - H - O^*Et \rightleftarrows EtO^*H + EtOH^*$	-	-	4.5×10^{-4}	equilibrium
(8)	$EtO^*H + EtOH^* \rightleftarrows Et - O^* - Et + *$	92	3.5×10^{12}	7.2×10^4	RDS
(9)	$Et - O^* - Et \rightleftarrows EtOEt + *$	-	-	1.3×10^{-6}	equilibrium

It is worthwhile mentioning a couple of works that complement the picture just outlined from an experimental point of view. Always within the framework of two parallel (unimolecular/bimolecular) routes from ethanol to ethylene or DEE, De Wilde et al. [76] worked with an alumina catalyst basically basically confirming the mechanism and the selectivity already described in [74]. They fitted their experimental data to a kinetic model that does not consider two types of active sites, but retains the water surface coverage as a rate-influencing parameter (Figure 14). This contribution, added to the theoretical calculations, seems then to indicate a different behavior of alumina and zeolites.

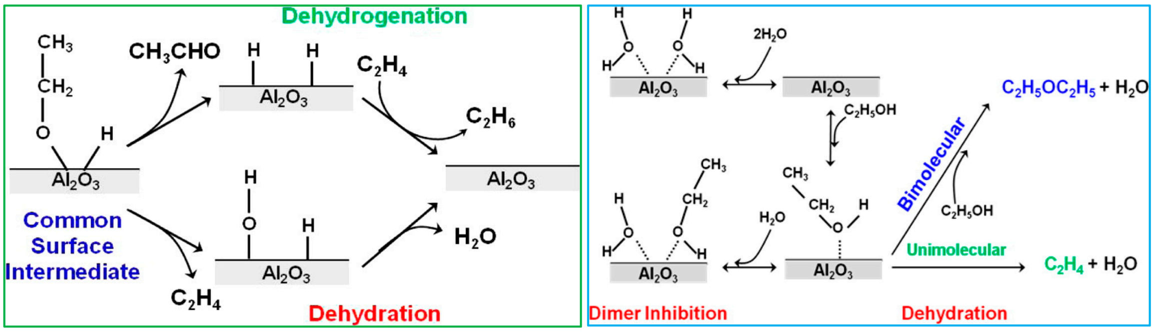

Figure 14. Reaction schemes outlined in references. Reproduced from [70]. Copyright 2014, ACS (**left**). Reproduced from [76]. Copyright 2013, ACS (**right**).

Afterwards DeWilde et al. [70] re-addressed from an experimental point of view the original discrimination between ethanol dehydration and dehydrogenation, applying also techniques of isotopic labeling and co-feeding pyridine alongside ethanol and water. The main finding of this work, besides the proposed re-hydrogenation of ethylene to ethane, can be summarized as follows: (i) at T > 600 K water is effectively desorbed from the catalyst, making the conversion rates again insensitive to its partial pressure; (ii) unimolecular reaction paths are kinetically determined by C–H breaks, while the DEE production is regulated by –O bonds cleavage; (iii) pyridine decreases the yield of both ethylene and acetaldehyde, confirming that the required –H abstraction step takes place on acidic sites.

This suggests that other factors, besides catalyst acidity, can be relevant in the possible yield of acetaldehyde also in ethanol dehydration reactions. Nevertheless, the ethylene production rate constant was given a kinetic pre-factor about 80 times larger than that of acetaldehyde [70], and this poses a substantial quantitative difference between these catalysts and the actually basic ones (e.g., Lanthana or Ceria—see for example the data on ethylene/acetaldehyde selectivity reported by [42].

The interplay between the ethylene/DEE reaction paths was lately reassessed by Knaeble and Iglesia [77], either experimentally (on acidic mixed metal catalyst supported on silica) and with a combined a priori (DFT based) heuristic calculation (Langmuir-Hinshelwood model with fitted parameters).

In building the mechanism schematically represented below (Figure 15), the authors did not only explain the deviation from unimolecular/bimolecular reaction rates just with varying catalyst coverages, but also with multiple contributions given by terms of different order: the resulting kinetic formulation is rather complex, but is rationalized into a model up to second order in ethanol partial pressure and six free parameters.

A complete DFT analysis of the relative transition states was contextually performed, and an "energetic profile" of the reaction was obtained as reproduced in Figure 16. The kinetic constants determined for the elementary steps were then statistically screened via a sensitivity analysis similar to the one mentioned above (i.e., examining the dependence of a certain yield on a small variation of the kinetic factors), since this considerably reduces the number of parameters actually needed for the model to account for the observed data.

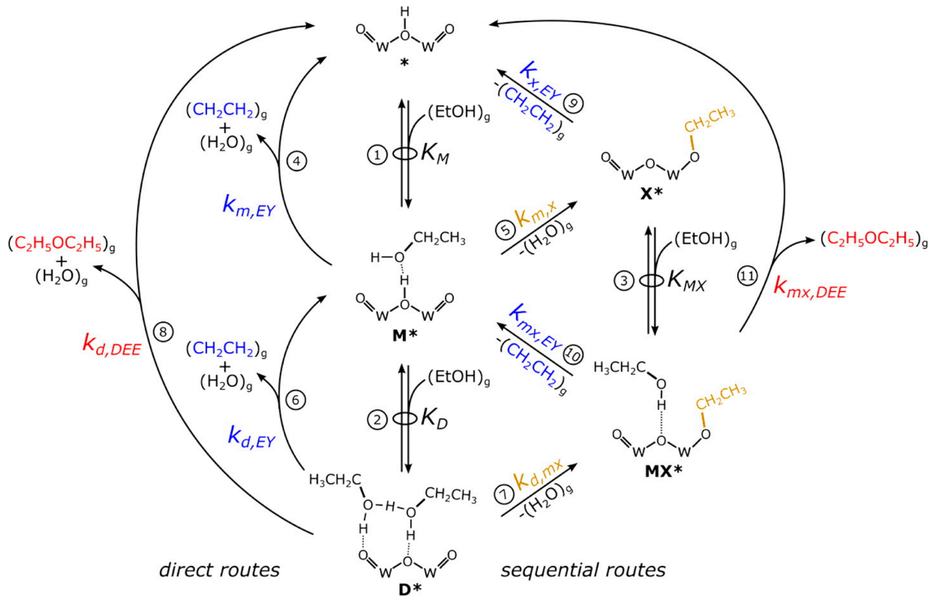

Figure 15. Reaction paths as traced in [77], built upon the catalyst regeneration cycle. Reproduced from [77]. Copyright 2016, ACS.

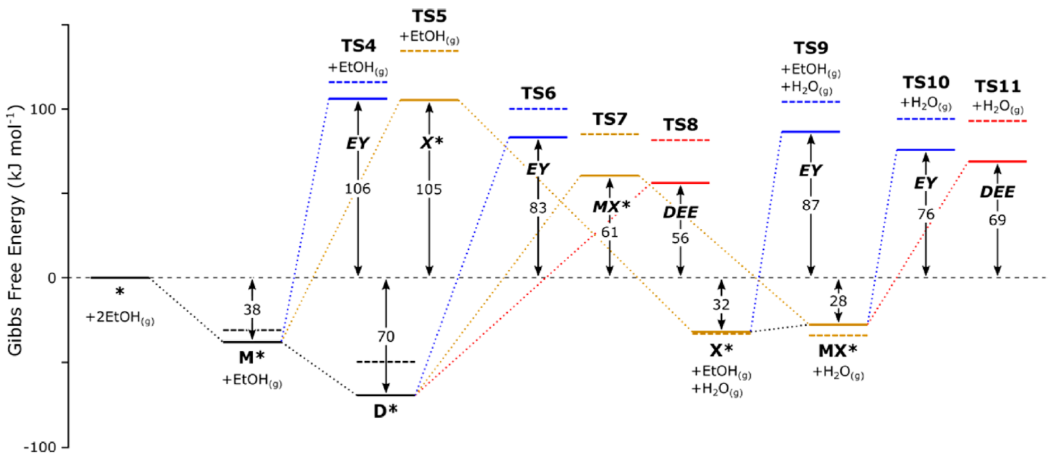

Figure 16. Gibbs free energy profile from reference [77], relative to mechanism reported in their Figure 7. Reproduced from [77]. Copyright 2016, ACS. (TS indicates the Transition State of the different steps defined in Figure 15).

After the selected kinetic parameters were adjusted to reproduce the observed data, they were compared with their bare values (i.e., those computed at the DFT level), and the same trends were found as a function of the energy required to exchange one H^+ unit between reactants and catalyst. As a result, the authors of the above work concluded that the bimolecular or concerted C–H and C–O breakings dominate for both ethylene and DEE production.

Up to this point, the selectivity issue seems to concern a minor yield of DEE, while it must be remembered that acidic catalysts do promote the polymerization of ethylene into aromatics or similar species of carbonaceous deposits [78]. Limiting to a theoretical analysis only, we mention as an example the DFT investigation of the fundamental step: $C_2H_4^* \rightarrow C_2H_5^{+\,*}$ reported in [74]. This protonation was chosen by the authors on the basis of several experimental works, so they could focus on the modeling of a few atomic configurations in order to compare the performance of two different materials (bare or P-doped HZSM5). This calculation shows that, since carbocation forms via a negative charge transfer along a $C^{\delta+}$–$O^{\delta-}$ bond (where the O atom binds the ethylene), if the adsorption occurs on an O–P site the transfer along the $C^{\delta+}$–$O^{\delta-}$–P route has a larger activation energy. This finding helps to rationalize on a firm ground the observed inhibition of coke in the presence of P inclusions.

Going then back to simpler semi-empirical accounts of the ethanol–ethylene reaction, there exist at least two works worth mentioning that propose relatively simple retro-fitting of lumped kinetic models to dedicated sets of data.

In the first [79], Kang et al. resorted to a Langmuir–Hinshelwood lumped model of the form:

$$r_{ethene} = k_{ethene} \frac{K_A P_{EtOH}}{1 + K_A P_{EtOH} + K_A K_{W1} P_{EtOH} P_{water} + K_{W2} P_{water}} \tag{9}$$

and set $K_{wi} \equiv 0$ for that temperature range (above 600 K) where effective water desorption makes the dehydration reaction insensitive to the product.

In the second [80], the authors obtained conversion data with a wider range of products on alumina, supporting the mechanism discussed above, but also confirming the hypothesis of DeWilde et al. on the possible acetaldehyde outcome. Indeed, this experimental work showed selectivity trends where ethylene and DEE appear as competitive paths, while ethylene and acetaldehyde could be on a common route. Though the proposed kinetics is oversimplified, the various product concentrations fitted fairly well to the model, probably because the selected reaction conditions make competitive adsorptions irrelevant. Moreover, a reactor model more complex than the ideal plug-flow one was used, treating thermal and mass transfer phenomena. We report here (Table 19) a comparison of the kinetic selectivity towards ethylene and DEE of some of the reviewed works.

Table 19. Data extracted from the cited works, for ethanol conversions obtained on alumina at 623 K.

Reference	**[79]**	**[70]**
Catalyst	**α-Alumina**	**γ-Alumina**
$\frac{k_{C_2H_4}}{k_{EtOEt}}$	$\frac{18\left(10^{-8} mol\ g_{cat}^{-1}\ s^{-1}\right)}{25\left(10^{-8} mol\ g_{cat}^{-1}\ s^{-1}\right)} = 0.72$	$\frac{9.4\left(10^{-4} mol\ g_{cat}^{-1}\ s^{-1}\right)}{6.8\left(10^{-4} mol\ g_{cat}^{-1}\ s^{-1}\right)} = 1.38$

In conclusion, we further mention a late DFT calculation [81] where the basic elimination mechanism (α–H abstraction from the C_α by the same alcoholic hydroxyl group) is set to work simultaneously in vacuum and on hematite surfaces modeled and oriented in different ways. Though not so extended in scope as the other reviewed works, this paper let one appreciate the fair compromise between accuracy, feasibility, and flexibility that a priori calculations have reached today—not to mention the potential interest of establishing ethylene production on cheap iron-based materials.

At the end, when the kinetic description of the process relies on a complex reactions set, mixed approaches can be considered in order to obtain all the needed kinetic and thermodynamic parameters. When possible, first principle study of the system can allow the independent determination of some parameters, whereas the other, kinetically relevant ones, can be regressed against proper experimental data. It is however strongly recommended to validate the calculated outcome against independent experimental data. In this way, it is generally possible to achieve reliable plant performance predictions on which process simulation can be safely carried out.

3. Conclusions

The present work outlines some case studies taken from process design and optimization, as well as from kinetic studies, which exemplify the use of process simulation tools. For a detailed and sound description of plant performance, the reactive steps have to be described with detailed kinetic models. Kinetic modelling is therefore one of the key steps in process development and it may be carried out either by developing detailed mechanistic microkinetic models, or by considering lumped/empirical approaches. In both cases, some indetermination may arise due to possible correlation between the regressed parameters, which ends in unreliable productivity predictions. First principle approaches to kinetic and thermodynamic description of reacting systems can be a valuable approach to limit such problems. Indeed, some of the parameters can be calculated independently, limiting the number of parameters to be regressed and therefore their correlation.

On this basis, process simulators allow the reliable description of full plant size provided that sufficiently reliable kinetic models are implemented. At first, kinetics of the studied reaction have to be inspected, deciding the level of detail that allows reliable interpretation of catalyst behavior and, thus, a credible process simulation. According to this choice, proper kinetic equation and the relative parameters must be available, to be implemented either in the default form imposed by the simulator, or by developing user models. When the complexity of the reaction network becomes too high, care must be put in the proper selection of the reaction set and in the evaluation of the reliability of the regressed kinetic parameters. In such cases, the user should evaluate the use of first principles to independently assess some of the parameters, so limiting the number of those, kinetically most relevant, to be regressed.

Author Contributions: M. Compagnoni and I. Rossetti. wrote Chapter 1; A. Tripodi and R. Martinazzo wrote the contributions in Chapter 2 on DFT and ab initio modelling; A. Tripodi, I. Rossetti and G. Ramis wrote the contribution on kinetics and process simulation in Chapter 2; I. Rossetti organized, revised and edited the paper.

Conflicts of Interest: The authors declare no conflict of interest.

References

1. Luyben, W.L. Design and Control of a Methanol Reactor/Column Process. *Ind. Eng. Chem. Res.* **2010**, *49*, 6150–6163. [CrossRef]
2. Vanden Bussche, K.M.; Froment, G.F. A Steady-State Kinetic Model for Methanol Synthesis and the Water Gas Shift Reaction on a Commercial $Cu/ZnO/Al_2O_3$Catalyst. *J. Catal.* **1996**, *161*, 1–10. [CrossRef]
3. Van-Dal, É.S.; Bouallou, C. Design and simulation of a methanol production plant from CO_2 hydrogenation. *J. Clean. Prod.* **2013**, *57*, 38–45. [CrossRef]
4. Lim, H.-W.; Park, M.-J.; Kang, S.-H.; Chae, H.-J.; Bae, J.W.; Jun, K.-W. Modeling of the kinetics for methanol synthesis using $Cu/ZnO/Al_2O_3<ZrO_2$ catalyst: Influence of carbon dioxide during hydrogenation. *Ind. Eng. Chem. Res.* **2009**, *48*, 10448–10455. [CrossRef]
5. Zhang, C.; Jun, K.W.; Gao, R.; Kwak, G.; Park, H.G. Carbon dioxide utilization in a gas-to-methanol process combined with CO_2/Steam-mixed reforming: Techno-economic analysis. *Fuel* **2017**, *190*, 303–311. [CrossRef]
6. Matzen, M.; Alhajji, M.; Demirel, Y. Chemical storage of wind energy by renewable methanol production: Feasibility analysis using a multi-criteria decision matrix. *Energy* **2015**, *93*, 343–353. [CrossRef]
7. Iyer, S.S.; Renganathan, T.; Pushpavanam, S.; Vasudeva, K.M.; Kaisare, N. Generalized thermodynamic analysis of methanol synthesis: Effect of feed composition. *J. CO_2 Util.* **2015**, *10*, 95–104. [CrossRef]
8. Rossetti, I.; Pernicone, N.; Ferrero, F.; Forni, L. Kinetic study of ammonia synthesis on a promoted Ru/C catalyst. *Ind. Eng. Chem. Res.* **2006**, *45*, 4150–4155. [CrossRef]
9. Rossetti, I.; Pernicone, N.; Forni, L. Graphitised carbon as support for Ru/C ammonia synthesis catalyst. *Catal. Today* **2005**, *102–103*, 219–224. [CrossRef]
10. Pernicone, N.; Ferrero, F.; Rossetti, I.; Forni, L.; Canton, P.; Riello, P.; Fagherazzi, G.; Signoretto, M.; Pinna, F. Wustite as a new precursor of industrial ammonia synthesis catalysts. *Appl. Catal. A Gen.* **2003**, *251*, 121–129. [CrossRef]
11. Rossetti, I.; Pernicone, N.; Forni, L. Promoters effect in Ru/C ammonia synthesis catalyst. *Appl. Catal. A Gen.* **2001**, *208*, 271–278. [CrossRef]
12. Yu, B.Y.; Chien, I.L. Design and Economic Evaluation of a Coal-Based Polygeneration Process to Coproduce Synthetic Natural Gas and Ammonia. *Ind. Eng. Chem. Res.* **2015**, *54*, 10073–10087. [CrossRef]
13. Arora, P.; Hoadley, A.F.A.; Mahajani, S.M.; Ganesh, A. Small-Scale Ammonia Production from Biomass: A Techno-Enviro-Economic Perspective. *Ind. Eng. Chem. Res.* **2016**, *55*, 6422–6434. [CrossRef]

14. Andersson, J.; Lundgren, J. Techno-economic analysis of ammonia production via integrated biomass gasification. *Appl. Energy* **2014**, *130*, 484–490. [CrossRef]
15. Aráujo, A.; Skogestad, S. Control structure design for the ammonia synthesis process. *Comput. Chem. Eng.* **2008**, *32*, 2920–2932. [CrossRef]
16. Mostafavi, E.; Sedghkerdar, M.H.; Mahinpey, N. Thermodynamic and Kinetic Study of CO_2 Capture with Calcium Based Sorbents: Experiments and Modeling. *Ind. Eng. Chem. Res.* **2013**, *52*, 4725–4733. [CrossRef]
17. Abdelouahed, L.; Authier, O.; Mauviel, G.; Corriou, J.P.; Verdier, G.; Dufour, A. Detailed Modeling of Biomass Gasi fi cation in Dual Fluidized Bed Reactors under Aspen Plus. *Energy Fuels* **2012**, *26*, 3840–3855. [CrossRef]
18. Rossetti, I.; Compagnoni, M.; De Guido, G.; Pellegrini, L.; Ramis, G.; Dzwigaj, S. Ethylene production from diluted bioethanol solutions. *Can. J. Chem. Eng.* **2017**. [CrossRef]
19. Rossetti, I.; Compagnoni, M.; Finocchio, E.; Ramis, G.; Di Michele, A.; Millot, Y.; Dzwigaj, S. Ethylene production via catalytic dehydration of diluted bioethanol: A step towards an integrated biorefinery. *Appl. Catal. B Environ.* **2017**, *210*, 407–420. [CrossRef]
20. Rossetti, I.; Compagnoni, M.; Finocchio, E.; Ramis, G.; Di Michele, A.; Zucchini, A.; Dzwigaj, S. Syngas production via steam reforming of bioethanol over Ni-BEA catalysts: A BTL strategy. *Int. J. Hydrogen Energy* **2016**, *41*, 16878–16889. [CrossRef]
21. Rossetti, I.; Biffi, C.; Tantardini, G.F.; Raimondi, M.; Vitto, E.; Alberti, D. 5 kW e + 5 kW t reformer-PEMFC energy generator from bioethanol first data on the fuel processor from a demonstrative project. *Int. J. Hydrogen Energy* **2012**, *37*, 8499–8504. [CrossRef]
22. Rossetti, I.; Compagnoni, M.; Torli, M. Process simulation and optimization of H_2 production from ethanol steam reforming and its use in fuel cells. 2. Process analysis and optimization. *Chem. Eng. J.* **2015**, *281*, 1036–1044. [CrossRef]
23. Rossetti, I.; Compagnoni, M.; Torli, M. Process simulation and optimization of H_2 production from ethanol steam reforming and its use in fuel cells. 1. Thermodynamic and kinetic analysis. *Chem. Eng. J.* **2015**, *281*, 1024–1035. [CrossRef]
24. Tripodi, A.; Compagnoni, M.; Rossetti, I. Kinetic modelling and reactor simulation for ethanol steam reforming. *ChemCatChem* **2016**, *8*, 3804–3813. [CrossRef]
25. Compagnoni, M.; Tripodi, A.; Rossetti, I. Parametric study and kinetic testing for ethanol steam refroming. *Appl. Catal. B Environ.* **2017**, *203*, 899–909. [CrossRef]
26. Oakley, J.H.; Hoadley, A.F.A. Industrial scale steam reforming of bioethanol: A conceptual study. *Int. J. Hydrog Energy* **2010**, *35*, 8472–8485. [CrossRef]
27. Khila, Z.; Hajjaji, N.; Pons, M.N.; Renaudin, V.; Houas, A. A comparative study on energetic and exergetic assessment of hydrogen production from bioethanol via steam reforming, partial oxidation and auto-thermal reforming processes. *Fuel Process. Technol.* **2013**, *112*, 19–27. [CrossRef]
28. Khila, Z.; Baccar, I.; Jemel, I.; Houas, A.; Hajjaji, N. Energetic, exergetic and environmental life cycle assessment analyses as tools for optimization of hydrogen production by autothermal reforming of bioethanol. *Int. J. Hydrogen Energy* **2016**, *41*, 17723–17739. [CrossRef]
29. Rossetti, I.; Biffi, C.; Forni, L.; Tantardini, G.F.; Faita, G.; Raimondi, M.; Vitto, E.; Alberti, D. Integrated 5 kWe + 5 kWt PEM-FC generator from bioethanol: A demonstrative project. In Proceedings of the ASME 2010 8th International Conference on Fuel Cell Science, Engineering and Technology (FUELCELL 2010), Brooklyn, NY, USA, 14–16 June 2010; Volume 2, pp. 465–471.
30. Rossetti, I.; Biffi, C.; Forni, L.; Tantardini, G.F.; Faita, G.; Raimondi, M.; Vitto, E.; Salogni, A. 5 KWE + 5 KWT PEM-FC generator from bioethanol: Fuel processor and development of new reforming catalysts. In Proceedings of the ASME 2011 9th International Conference on Fuel Cell Science, Engineering and Technology, Grand, Hyatt, DC, USA, 7–11 August 2011; pp. 47–53.
31. Rossetti, I.; Lasso, J.; Compagnoni, M.; De Guido, G.; Pellegrini, L. H_2 production from bioethanol and its use in fuel-cells. *Chem. Eng. Trans.* **2015**, *43*, 229–234. [CrossRef]
32. Francesconi, J.A.; Mussati, M.C.; Mato, R.O.; Aguirre, P.A. Analysis of the energy efficiency of an integrated ethanol processor for PEM fuel cell systems. *J. Power Sources* **2007**, *167*, 151–161. [CrossRef]
33. Jaggi, V.; Jayanti, S. A conceptual model of a high-efficiency, stand-alone power unit based on a fuel cell stack with an integrated auto-thermal ethanol reformer. *Appl. Energy* **2013**, *110*, 295–303. [CrossRef]
34. Aicher, T.; Full, J.; Schaadt, A. A portable fuel processor for hydrogen production from ethanol in a 250 Wel fuel cell system. *Int. J. Hydrogen Energy* **2009**, *34*, 8006–8015. [CrossRef]

35. Nieto, D.L.; Biset, S.; Luppi, P.; Basualdo, M.S. A rigorous computational model for hydrogen production from bio-ethanol to feed a fuel cell stack. *Int. J. Hydrogen Energy* **2012**, *37*, 3108–3129. [CrossRef]
36. Nieto Degliuomini, L.; Zumoffen, D.; Basualdo, M. Plant-wide control design for fuel processor system with PEMFC. *Int. J. Hydrogen Energy* **2012**, *37*, 14801–14811. [CrossRef]
37. Stefan, M.; Wörner, A. On-board reforming of biodiesel and bioethanol for high temperature PEM fuel cells: Comparison of autothermal reforming and steam reforming. *J. Power Sources* **2011**, *196*, 3163–3171. [CrossRef]
38. Gutiérrez, G.N.; Jiménez, V.M.; Serrano-Ruiz, J.C.; de Lucas-Consuegra, A. Electrochemical reforming vs. Catalytic reforming of ethanol: A process energy analysis for hydrogen production. *Chem. Eng. Process. Process Intensif.* **2015**, *95*, 9–16. [CrossRef]
39. Wang, C.B.; Lee, C.C.; Bi, J.L.; Siang, J.Y.; Liu, J.Y.; Yeh, C.T. Study on the steam reforming of ethanol over cobalt oxides. *Catal. Today* **2009**, *146*, 76–81. [CrossRef]
40. Vaidya, P.D.; Rodrigues, A.E. Insight into steam reforming of ethanol to produce hydrogen for fuel cells. *Chem. Eng. J.* **2006**, *117*, 39–49. [CrossRef]
41. Casanovas, A.; Roig, M.; De Leitenburg, C.; Trovarelli, A.; Llorca, J. Ethanol steam reforming and water gas shift over Co/ZnO catalytic honeycombs doped with Fe, Ni, Cu, Cr and Na. *Int. J. Hydrogen Energy* **2010**, *35*, 7690–7698. [CrossRef]
42. Fatsikostas, A.N.; Verykios, X.E. Reaction network of steam reforming of ethanol over Ni-based catalysts. *J. Catal.* **2004**, *225*, 439–452. [CrossRef]
43. Díaz, A.F.; Gracia, F. Steam reforming of ethanol for hydrogen production: Thermodynamic analysis including different carbon deposits representation. *Chem. Eng. J.* **2010**, *165*, 649–657. [CrossRef]
44. Mas, V.; Kipreos, R.; Amadeo, N.; Laborde, M. Thermodynamic analysis of ethanol/water system with the stoichiometric method. *Int. J. Hydrogen Energy* **2006**, *31*, 21–28. [CrossRef]
45. Vaidya, P.D.; Rodrigues, A.E. Kinetics of steam reforming of ethanol over a Ru/Al_2O_3 catalyst. *Ind. Eng. Chem. Res.* **2006**, *45*, 6614–6618. [CrossRef]
46. Mathure, P.V.; Ganguly, S.; Patwardhan, A.V.; Saha, R.K. Steam reforming of ethanol using a commercial nickel-based catalyst. *Ind. Eng. Chem. Res.* **2007**, *46*, 8471–8479. [CrossRef]
47. Akande, A.; Aboudheir, A.; Idem, R.; Dalai, A. Kinetic modeling of hydrogen production by the catalytic reforming of crude ethanol over a CO–Precipitated Ni-Al_2O_3 catalyst in a packed bed tubular reactor. *Int. J. Hydrogen Energy* **2006**, *31*, 1707–1715. [CrossRef]
48. Birot, A.; Epron, F.; Descorme, C.; Duprez, D. Ethanol steam reforming over Rh/$CexZ_{r1-x}O_2$ catalysts: Impact of the CO-CO_2-CH_4 interconversion reactions on the H_2 production. *Appl. Catal. B Environ.* **2008**, *79*, 17–25. [CrossRef]
49. Comas, J.; Marino, F.; Laborde, M.; Amadeo, N. Bio-ethanol steam reforming on Ni/Al_2O_3 catalyst. *Chem. Eng. J.* **2004**, *98*, 61–68. [CrossRef]
50. Cavallaro, S. Ethanol Steam Reforming on Rh/Al_2O_3 Catalysts. *Energy* **2000**, 1195–1199. [CrossRef]
51. Wang, F.; Cai, W.; Descorme, C.; Provendier, H.; Shen, W.; Mirodatos, C.; Schuurman, Y. From mechanistic to kinetic analyses of ethanol steam reforming over Ir/CeO_2 catalyst. *Int. J. Hydrogen Energy* **2014**, *39*, 18005–18015. [CrossRef]
52. Mas, V.; Bergamini, M.L.; Baronetti, G.; Amadeo, N.; Laborde, M. A kinetic study of ethanol steam reforming using a nickel based catalyst. *Top. Catal.* **2008**, *51*, 39–48. [CrossRef]
53. Llera, I.; Mas, V.; Bergamini, M.L.; Laborde, M.; Amadeo, N. Bio-ethanol steam reforming on Ni based catalyst. Kinetic study. *Chem. Eng. Sci.* **2012**, *71*, 356–366. [CrossRef]
54. Graschinsky, C.; Laborde, M.; Amadeo, N.; Le Valant, A.; Blon, N.; Epron, F.; Duprez, D. Ethanol steam reforming over Rh/Al: A kinetic study. *Eng. Chem. Res.* **2010**, *49*. [CrossRef]
55. Sahoo, D.R.; Vajpai, S.; Patel, S.; Pant, K.K. Kinetic modeling of steam reforming of ethanol for the production of hydrogen over Co/Al_2O_3 catalyst. *Chem. Eng. J.* **2007**, *125*, 139–147. [CrossRef]
56. Görke, O.; Pfeifer, P.; Schubert, K. Kinetic study of ethanol reforming in a microreactor. *Appl. Catal. A Gen.* **2009**, *360*, 232–241. [CrossRef]
57. Simson, A.; Waterman, E.; Farrauto, R.; Castaldi, M. Kinetic and process study for ethanol reforming using a Rh/Pt washcoated monolith catalyst. *Appl. Catal. B Environ.* **2009**, *89*, 58–64. [CrossRef]
58. Bruschi, Y.M.; López, E.; Schbib, N.S.; Pedernera, M.N.; Borio, D.O. Theoretical study of the ethanol steam reforming in a parallel channel reactor. *Int. J. Hydrogen Energy* **2012**, *37*, 14887–14894. [CrossRef]

59. Cunha, A.F.; Wu, Y.J.; Santos, J.C.; Rodrigues, A.E. Steam Reforming of Ethanol on Copper Catalysts Derived from Hydrotalcite-like Materials. *Ind. Eng. Chem. Res.* **2012**, *51*, 13132–13143. [CrossRef]
60. Cunha, A.F.; Wu, Y.J.; Li, P.; Yu, J.G.; Rodrigues, A.E. Sorption-enhanced steam reforming of ethanol on a novel K-Ni-Cu-hydrotalcite hybrid material. *Ind. Eng. Chem. Res.* **2014**, *53*, 3842–3853. [CrossRef]
61. Wu, Y.J.; Li, P.; Yu, J.G.; Cunha, A.F.; Rodrigues, A.E. Sorption-enhanced steam reforming of ethanol on NiMgAl multifunctional materials: Experimental and numerical investigation. *Chem. Eng. J.* **2013**, *231*, 36–48. [CrossRef]
62. Wu, Y.J.; Li, P.; Yu, J.G.; Cunha, A.F.; Rodrigues, A.E. Sorption-enhanced steam reforming of ethanol for continuous high-purity hydrogen production: 2D adsorptive reactor dynamics and process design. *Chem. Eng. Sci.* **2014**, *118*, 83–93. [CrossRef]
63. Fierro, V.; Akdim, O.; Provendier, H.; Mirodatos, C. Ethanol oxidative steam reforming over Ni-based catalysts. *J. Power Sources* **2005**, *145*, 659–666. [CrossRef]
64. Mondal, T.; Pant, K.K.; Dalai, A.K. Mechanistic Kinetic Modeling of Oxidative Steam Reforming of Bioethanol for Hydrogen Production over Rh–Ni/CeO_2–ZrO_2 Catalyst. *Ind. Eng. Chem. Res.* **2016**, *55*, 86–98. [CrossRef]
65. Wang, J.H.; Lee, C.S.; Lin, M.C. Mechanism of ethanol reforming: Theoretical foundations. *J. Phys. Chem. C* **2009**, *113*, 6681–6688. [CrossRef]
66. Nørskov, J.K.; Bligaard, T.; Rossmeisl, J.; Christensen, C.H. Towards the computational design of solid catalysts. *Nat. Chem.* **2009**, *1*, 37–46. [CrossRef] [PubMed]
67. Sutton, J.E.; Vlachos, D.G. Ethanol Activation on Closed-Packed Surfaces. *Ind. Eng. Chem. Res.* **2015**, *54*, 4213–4225. [CrossRef]
68. Sutton, J.E.; Panagiotopoulou, P.; Verykios, X.E.; Vlachos, D.G. Combined DFT, microkinetic, and experimental study of ethanol steam reforming on Pt. *J. Phys. Chem. C* **2013**, *117*, 4691–4706. [CrossRef]
69. Koehle, M.; Mhadeshwar, A. Microkinetic modeling and analysis of ethanol partial oxidation and reforming reaction pathways on platinum at short contact times. *Chem. Eng. Sci.* **2012**, *78*, 209–225. [CrossRef]
70. DeWilde, J.F.; Czopinski, C.J.; Bhan, A. Ethanol dehydration and dehydrogenation on Al_2O_3: Mechanism of acetaldehyde formation. *ACS Catal.* **2014**, *4*, 4425–4433. [CrossRef]
71. Dumrongsakda, P.; Ruangpornvisuti, V. Theoretical investigation of ethanol conversion to ethylene over H-ZSM-5 and transition metals-exchanged ZSM-5. *Catal. Lett.* **2012**, *142*, 143–149. [CrossRef]
72. Kim, S.; Robichaud, D.J.; Beckham, G.T.; Paton, R.S.; Nimlos, M.R. Ethanol dehydration in HZSM-5 studied by density functional theory: Evidence for a concerted process. *J. Phys. Chem. A* **2015**, *119*, 3604–3614. [CrossRef] [PubMed]
73. Maihom, T.; Khongpracha, P.; Sirijaraensre, J.; Limtrakul, J. Mechanistic studies on the transformation of ethanol into ethene over Fe-ZSM-5 zeolite. *ChemPhysChem* **2013**, *14*, 101–107. [CrossRef] [PubMed]
74. Christiansen, M.A.; Mpourmpakis, G.; Vlachos, D.G. DFT-driven multi-site microkinetic modeling of ethanol conversion to ethylene and diethyl ether on γ-Al_2O_3(111). *J. Catal.* **2015**, *323*, 121–131. [CrossRef]
75. Alexopoulos, K.; John, M.; Van der Borght, K.; Galvita, V.; Reyniers, M.; Marin, G.B. DFT-based microkinetic modeling of ethanol dehydration in H-ZSM-5. *J. Catal.* **2016**, *339*, 173–185. [CrossRef]
76. DeWilde, J.F.; Chiang, H.; Hickman, D.A.; Ho, C.R.; Bhan, A. Kinetics and mechanism of ethanol dehydration on Al_2O_3: The critical role of dimer inhibition. *ACS Catal.* **2013**, *3*, 798–807. [CrossRef]
77. Knaeble, W.; Iglesia, E. Kinetic and Theoretical Insights into the Mechanism of Alkanol Dehydration on Solid Brønsted Acid Catalysts. *J. Phys. Chem. C* **2016**, *120*, 3371–3389. [CrossRef]
78. Bartholomew, C.H. Mechanisms of catalyst deactivation. *Appl. Catal. A Gen.* **2001**, *212*, 17–60. [CrossRef]
79. Kang, M.; Bhan, A. Kinetics and mechanisms of alcohol dehydration pathways on alumina. *Catal. Sci. Technol.* **2016**, *6*, 6667–6678. [CrossRef]
80. Kagyrmanova, A.P.; Chumachenko, V.A.; Korotkikh, V.N.; Kashkin, V.N.; Noskov, A.S. Catalytic dehydration of bioethanol to ethylene: Pilot-scale studies and process simulation. *Chem. Eng. J.* **2011**, *176–177*, 188–194. [CrossRef]
81. Lopes, J.F.; Silva, J.C.M.; Cruz, M.T.M.; De Carneiro, J.W.M.; De Almeida, W.B. DFT study of ethanol dehydration catalysed by hematite. *RSC Adv.* **2016**, *6*, 40408–40417. [CrossRef]